OPEN ACCESS
phytobiomesjournal.org
Phytobiomes Journal
A Transdisciplinary Journal of Sustainable Plant Productivity

RESEARCH

Diverse *Pseudomonas* Species Engage in Beneficial and Suppressive Interactions with the Kiwifruit Pathogen *Pseudomonas syringae* pv. *actinidiae* Across *Actinidia* Germplasm

Haileigh R. Patterson,[1,2] Lauren M. Hemara,[1,2] Matthew D. Templeton,[1,2,3] and Jay Jayaraman[2,†]

[1] School of Biological Sciences, The University of Auckland, Auckland, New Zealand
[2] Plant and Food Research Group, New Zealand Institute for Bioeconomy Science, Mt. Albert, Auckland, New Zealand
[3] Bioprotection Aotearoa, Lincoln University, Lincoln, New Zealand

Accepted for publication 19 December 2025.

Abstract

In 2010, a *Pseudomonas syringae* pv. *actinidiae* biovar 3 (Psa3) incursion into New Zealand devastated susceptible kiwifruit (*Actinidia chinensis*) orchards. In contrast, many *Actinidia* species maintained in germplasm collections were Psa3-resistant and showed limited symptoms. However, recent genome biosurveillance revealed the emergence of widespread leaf spot symptoms in *Actinidia* germplasm. Psa3 isolates were recovered from only 12% of symptomatic tissue collected, despite the frequent isolation of phenotypical *Pseudomonas* isolates on selective agar. Despite the poor recovery of Psa3 isolates, Psa3 was found in all symptomatic tissue through qPCR and metabarcoding analysis. Metabarcoding revealed stark differences in bacterial community composition from samples taken from symptomatic or lesion-free tissue from the same leaf. Host genotype also influenced community composition, but to a lesser extent. Whole-genome sequencing of 15 diverse *Pseudomonas* isolates revealed that many belonged to the *P. syringae* species complex. Curiously, the kiwifruit-associated *P. syringae* pv. *actinidifoliorum* (Pfm) was never recovered. Pathogenicity and competitive assays revealed that although individually these *Pseudomonas* isolates were not more pathogenic than Pfm or Psa3 on resistant *Actinidia* hosts, some could interact with Psa3 to improve their growth, suggesting that these isolates may form pathogenic consortia in these disease-associated phyllosphere communities on typically Psa3-resistant hosts.

Keywords: consortia, microbiome, mutualism, plant pathology

[†]Corresponding author: J. Jayaraman; jay.jayaraman@plantandfood.co.nz

Author contributions: H.R.P. curated the data, conducted the formal analysis and investigation, developed the methodology, performed the project administration, provided the software, conducted the validation and visualization, wrote the original draft of the manuscript, and reviewed and edited the manuscript. L.M.H. conceptualized the study, curated the data, conducted the formal analysis and investigation, developed the methodology, performed the project administration, provided the software, supervised the study, conducted the validation and visualization, wrote the original draft of the manuscript, and reviewed and edited the manuscript. J.J. conceptualized the study, acquired the funding, developed the methodology, performed the project administration, supervised the study, and reviewed and edited the manuscript. M.D.T. curated the data, acquired the funding, supervised the study, and reviewed and edited the manuscript.

H. R. Patterson and L. M. Hemara share first authorship on this work.

Current address for L. M. Hemara: Department of Physical & Environmental Sciences, University of Toronto Scarborough, Toronto, Ontario, Canada.

Data availability: Sequence data are available in the GenBank Nucleotide Database (https://www.ncbi.nlm.nih.gov/genbank/) and Sequence Read Archive (https://www.ncbi.nlm.nih.gov/sra) under BioProject PRJNA1213159 and PRJNA1398373.

The phyllosphere is one of the most abundant and diverse habitats in the world, host to commensal and mutualistic epiphytes, as well as phytopathogens transitioning from epiphytic to endophytic lifestyles (Cook et al. 2015; Drew et al. 2021; Vorholt 2012). Bacteria are the most abundant inhabitants of the phyllosphere (Leveau 2006; Lindow and Brandl 2003; Peñuelas and Terradas 2014), although the leaf surface is also occupied by a wide range of prokaryotic and eukaryotic microorganisms (Sohrabi et al. 2023). The phyllosphere differs from the widely studied rhizosphere, as each leaf is exposed to the environment, where colonization can be short-lived and adaptations to harsh conditions are paramount (Lindow and Brandl 2003; Vorholt 2012). Further still, each leaf is a microclimate that experiences temperature, water, light, and humidity fluctuations, punctuated by plant architecture of trichomes and stomata (Vacher et al. 2016). Phyllosphere bacteria, therefore,

Funding: Support was provided by the Marsden Fund (MFP-PAF2001).

e-Xtra: Supplementary material is available online.

The author(s) declare no conflict of interest.

often exist in multispecies aggregates to protect themselves from harsh conditions on the leaf surface (Vorholt 2012). The exposure of leaf surfaces to the environment not only selects for certain microbes but also means the possibilities for bacterial introduction are greater, through both endophytic and external colonization pathways, such as the seed and rhizosphere microbiome, biological vectors (including insects), and abiotic factors such as wind and rain (Bulgarelli et al. 2013; Morris 2002; Vacher et al. 2016).

Bacteria in the phyllosphere can be considered through two lenses: the way they interact with the plants they live on (host–microbe interactions), and how they interact with other inhabitants of the phyllosphere (microbe–microbe interactions). Within host–microbe interactions, bacteria exist on a spectrum of mutualism to pathogenicity, along which they may transit (Cook et al. 2015; Drew et al. 2021; Vorholt 2012). Regardless of where bacteria sit on the symbiosis spectrum, they share common strategies for symbiosis, including motility, chemotaxis, and metabolic adaptations for both competition and host immune suppression (Wiesmann et al. 2022). Much like host–microbe interactions, microbe–microbe interactions can also exist on a spectrum of interactions, as mutualism, co-virulence, and competition may occur simultaneously within the phyllosphere. For example, phyllosphere bacteria can form pathogenic consortia, altering disease severity and bacterial growth dynamics (Sadhukhan et al. 2024). In the field, the intersection of host–microbe and microbe–microbe interactions is likely to be complex and, to date, is poorly understood. However, recent work has begun to elucidate the key roles and mechanisms of the phyllosphere microbiome in disease (Chen et al. 2020; Paasch et al. 2023; Su et al. 2024).

Pseudomonas syringae is one of the most widely studied phyllosphere bacteria owing to its ubiquitous and often pathogenic nature (Chaudhry et al. 2021; Diallo et al. 2012; Hirano and Upper 2000). In particular, members of the *P. syringae* species complex cause disease more frequently than any other bacterial species, often implicated in new epidemics and posing a major threat to food production globally (Morris et al. 2019). Like other phytopathogens, *P. syringae*'s virulence strategy includes the secretion of effectors and toxins into host cells, which facilitate pathogen entry into the host, suppress host defenses, promote pathogen proliferation in host tissue, and aid in nutrient acquisition (Xin et al. 2018). However, many *P. syringae* also have beneficial or neutral interactions with plant hosts and can be found ubiquitously in the environment as part of the water cycle (Morris et al. 2008). Additionally, closely related strains may also be on opposite ends of this spectrum, such as commensal *P. fluorescens* isolates that protect *Arabidopsis thaliana* from genetically similar pathogenic isolates (Wang et al. 2022). This makes *P. syringae* particularly interesting to study, as it represents both established and potential pathogens, allowing us to decipher what may drive new incursions and the evolution of pathogenesis.

In 2010, *P. syringae* pv. *actinidiae* biovar 3 (Psa3) was isolated from kiwifruit vines in New Zealand (Everett et al. 2011). In susceptible hosts, Psa3 causes necrotic leaf spots, cane canker, vine dieback, bud rot, and flower wilting, often leading to the loss of entire vines. Psa3 caused significant financial losses and changed the landscape of kiwifruit production. In the years since this global Psa pandemic, extensive research has been undertaken to understand the origins, virulence, and evolution of the economically important pathogen (Butler et al. 2013; Cellini et al. 2021, 2022; Colombi et al. 2017; Donati et al. 2020; Hemara et al. 2022, 2025a; Ishiga et al. 2023; Jayaraman et al. 2020, 2023; McAtee et al. 2018; McCann et al. 2013, 2017; Michelotti et al. 2018; Poulter et al. 2018; Sawada and Fujikawa 2019; Vlková-Žlebková et al. 2024; Warring et al. 2022; Zhao et al. 2019). Despite considerable contemporary understanding of Psa, knowledge about the larger context and communities in which it exists is only now being revealed. For instance, several *Pseudomonas* spp. can cause symptoms on kiwifruit, including *P. viridiflava*, *P. syringae* pv. *syringae* (Pss), and *P. syringae* pv. *actinidifoliorum* (Pfm; Cunty et al. 2015; González et al. 2024; Visnovsky et al. 2019), yet little is known about how these might interact in planta. The Psa–kiwifruit pathosystem thus presents an opportunity to examine these interactions in the field across diverse, co-located host genotypes in *Actinidia* germplasm collections (Hemara et al. 2022, 2025a). Diverse *Actinidia* species have differing degrees of susceptibility or resistance to Psa3. Whereas commercial *Actinidia chinensis* cultivars grown in monoculture are considered susceptible or tolerant, members of the *Leiocarpae* section of the *Actinidia* genus show resistance to Psa, with only select individuals from *A. arguta*, *A. macrosperma*, *A. valvata*, *A. polygama*, and *A. melanandra* removed from New Zealand germplasm collections because of Psa infection (Datson et al. 2015; Liu et al. 2017). In particular, *A. arguta* and *A. melanandra* are known to recognize Psa through strong effector-triggered immune responses (Hemara et al. 2022, 2025a). Although these species are not grown in large-scale commercial monocultures, they represent a wealth of genetic diversity in the *Actinidia* germplasm collections used for new cultivar development.

Following the establishment of Psa3 in New Zealand, a comprehensive genome biosurveillance program was developed to monitor the evolution of Psa3 over time and to anticipate changes in virulence (Hemara et al. 2022, 2025a, b). Although the molecular basis for Psa3's pathogenicity is well understood (Asif et al. 2025; Cellini et al. 2021, 2022; Donati et al. 2020; Ishiga et al. 2023; Jayaraman et al. 2020, 2023; McCann et al. 2013; Straub et al. 2018; Zhang et al. 2022; Zhao et al. 2019), little is known about how this pathogen may be interacting with other phyllosphere microbes, and even less about what constitutes the phyllosphere microbiome in *Actinidia* species outside of commercial monoculture. Sampling symptomatic plant material from *Actinidia* germplasm collections held at Plant & Food Research sites remains a key aspect of Psa surveillance efforts, tracking evolution outside commercial orchard settings. In this work, this genome biosurveillance program was leveraged to investigate more diverse *Pseudomonas* spp. isolated from the phyllosphere of symptomatic leaves from germplasm collections. In doing so, the following questions were addressed: What constitutes the bacterial community of diverse *Actinidia* species? What are the factors influencing community composition? Do the microbes associated with diverse *Actinidia* hosts cause the observed symptoms? Can the resident microbes on germplasm *Actinidia* form pathogenic consortia with Psa to increase disease? Alternatively, can these phyllosphere microbes form suppressive communities that reduce disease incidence or severity?

Materials and Methods

Germplasm sampling

Two kiwifruit germplasm collections held at Plant & Food Research's Kerikeri and Te Puke research orchards were sampled. Each comprised multiple blocks of diverse, unimproved *Actinidia* spp. vines, grown from kiwifruit seeds collected from the wild in China (Richardson et al. 2023). Symptomatic leaves were collected from Te Puke and Kerikeri in December 2022. Two hundred and thirty-three samples were taken from 134 accessions representing 18 species of *Actinidia*. At least two leaves were sampled per vine, and vines were selected for sampling to represent all *Actinidia* species displaying leaf spot symptoms. Gloves and tools were sanitized using 80% ethanol between vines. Leaves sampled at Te Puke were stored in insulated boxes with ice packs for transport back

to Bioeconomy Science Institute's Mount Albert Research Centre (MARC) and held overnight at 4°C before processing the next day. Leaves sampled at Kerikeri were kept ambient during sampling and stored at 4°C overnight at Kerikeri. They were then transported back to MARC in insulated cold boxes and stored overnight at 4°C before processing the next day. Samples were processed 1 to 2 days postharvest. Leaves were photographed, and the features of visible lesions were noted. From the 233 leaf samples taken, 199 symptomatic and 119 asymptomatic leaf discs were processed into leaf homogenate for analysis to avoid duplicate genotype representation.

Symptomatic leaf discs were taken from visible lesions, whereas asymptomatic leaf discs were sampled from visually asymptomatic portions of the same leaf. For each sample, up to four leaf discs were taken using a 5-mm cork-borer from either symptomatic or asymptomatic portions of leaf. Leaf discs were immediately submerged in 350 µl of sterile 10 mM $MgSO_4$ with three stainless steel beads. Tools and surfaces were sterilized with 70% ethanol between each sample. Samples were homogenized using a Storm24 Bullet Blender (Next Advance, Troy, NY, U.S.A.) at speed 12 for 2 min. An additional 350 µl of $MgSO_4$ was added, and the homogenization was repeated. Leaf homogenate was stored at −20°C prior to DNA extraction.

Amplicon sequencing

Sample selection. A total of 74 samples were selected for amplicon sequencing: 37 symptomatic and 37 corresponding asymptomatic samples (Supplementary Table S1). Samples were selected to represent every *Actinidia* species, with equal representation across both sites where possible. Priority was given to species that are retained in tissue culture by Plant & Food Research, for downstream continuity of in planta assays. These included *A. polygama*, *A. melanandra*, and *A. arguta*. Within these species, a range of genotypes were selected, where possible. Two sterile tissue culture samples (*A. arguta* AA07_03 and *A. polygama* PC02_01) were also included in the amplicon sequencing as negative controls, along with a sterile water nontemplate control. Along with the phyllosphere samples, we included a ZymoBIOMICS Microbial Community Standard (Zymo Research, Irvine, CA, U.S.A.) as a "mock" community control for read depth and accuracy and a sample of Psa V-13 genomic DNA (gDNA) as a positive control.

DNA extraction. A QIAGEN DNeasy Plant Mini Kit (QIAGEN, Hilden, Germany) was used to extract DNA from leaf samples for 16S amplicon sequencing. The kit was used according to the manufacturer's provided quick-start protocol. Nontemplate controls were used for all extractions and later were screened for contamination with qPCR utilizing Psa-specific and universal bacterial internal transcribed spacer primers. DNA was then stored at 4°C.

Quantitative PCR (qPCR). qPCR was used to ascertain bacterial presence in the samples selected for amplicon sequencing and to test for the presence of Psa. Psa F1/R2 primers specific to Psa and Pfm were used (Rees-George et al. 2010), as well as "universal" 335F/769R primers for amplifying bacterial 16S rRNA gene regions (Supplementary Table S2; Dorn-In et al. 2015). Plant reference gene (EF1α) primers, SN126L/R (Nardozza et al. 2013), were used for normalization. The primers used to identify nonspecific bacterial presence by qPCR, 335F/769R, were shown to have an efficiency of 102% and an amplification factor of 2.02. Nontemplate controls were used for all runs with each primer pair, with wild-type Psa3 V-13 gDNA used as a positive control. A qPCR was performed using an Illumina Eco Real-Time PCR System. The qPCR parameters were based on previous work by Andersen et al. (2018), using SsoAdvanced Universal SYBR Green Supermix (Bio-Rad, Hercules, CA, U.S.A.).

End-point PCR and sequencing. End-point PCR was performed in 50-µl reactions in 0.2-ml PCR tubes. Master mixes were made fresh for each run and aliquoted into tubes, followed by template DNA (Supplementary Table S3). End-point PCRs were conducted in an Eppendorf Mastercycler X50I thermal cycler (Eppendorf, Hamburg, Germany) using the parameters outlined in Supplementary Table S4. Symptomatic phyllosphere samples were amplified for 30 PCR cycles, and asymptomatic samples were amplified for 40 PCR cycles. The ZymoBIOLOMICS Microbial Community Standard and Psa3 V-13 gDNA controls were amplified for 30 cycles. The no-template control, a "blank" sample that went through all extraction processes, was amplified for 40 cycles.

Samples were amplified (using the conditions listed above) with the 16S rRNA V5-V9 primers 799F (AACMGGATTAGATA CCCKG) and 1492R (TACGGYTACCTTGTTACGACTT), generating an approximately 690-bp product. Samples were prepared with AMPure XP (Beckman Coulter Life Sciences, Brea, CA, U.S.A.) bead clean-up. Amplicon concentration was quantified with Qubit (Thermo Fischer Scientific, Waltham, MA, U.S.A.) and normalized to approximately 5 ng/µl.

Nanopore sequencing was performed using an SQK-LSK114 Ligation Sequencing Kit with EXP-PBC096 barcoding on a PromethION FLO-PRO114M flowcell through Auckland Genomics (University of Auckland, Auckland, New Zealand). Real-time base-calling was done using a high-accuracy model with Guppy 7.1.4. Adaptors were trimmed, but barcodes were not. After the run was complete, the reads were "re-base-called" using a super-high-accuracy model with Dorado 0.5.3 and model dna_r10.4.1_e8.2_400bps_sup@v4.2.0. Quality checking of sequences was performed with FastQC (Andrews et al. 2010) and MultiQC (Ewels et al. 2016).

Bioinformatic and statistical analysis. Data analysis was conducted in R (version 4.2.1; R Core Team 2024). 16S amplicon sequencing reads were processed into amplicon sequence variants (ASVs) using the R package 'dada2' (version 1.24.0; Callahan et al. 2016). ONT reads were treated as single-end reads and were filtered for quality, using relaxed maxEE values (maxEE = 15, truncQ = 2, minLen = 400, maxLen = 1,000). Taxonomy was assigned to the genus level using the SILVA v.132 database for both forward and reverse-complement orientations (tryRC = TRUE, minBoot = 80), with further species-level assignments made based on exact matching to reference sequences. The R package 'decontam' was used to identify contaminant ASVs for removal that were present in no-template control samples (version 1.18.0; Davis et al. 2018). The R package 'phyloseq' (version 1.42.0; McMurdie and Holmes 2013) was used to create a phyloseq object of metadata and count data, perform ordination, and visualize results. Each sample was normalized to the median sequencing depth (https://joey711.github.io/phyloseq/preprocess.html). Taxonomy was visualized at the genus and species levels (where applicable) using the plot_bar() function (McMurdie and Holmes 2013). The merge_samples2() function from the 'speedyseq' package was used to visualize relative abundance by data levels (version 0.2.0; https://github.com/mikemc/speedyseq). Alpha and beta diversity were calculated as laid out in the meta-analysis pipeline from Hoffbeck et al. (2023). The plot_richness() function was used to calculate alpha diversity using the Shannon diversity metric (McMurdie and Holmes 2013). The ordinate() function was used to calculate beta diversity using a Bray–Curtis dissimilarity matrix (McMurdie and Holmes 2013). Permutational multivariate analysis of variance statistical significance was calculated using Bray–Curtis dissimilarity with 9,999 permutations using the adonis() function from the 'vegan' package (version 2.6-2; Oksanen et al. 2024). *Pseudomonas* ASVs were identified to the species or subspecies level through BLASTn

and comparison with reference sequences (Johnson et al. 2008). The core_members() function from the microbiome package was used to identify core members of the microbiome (80% core threshold; version 1.20.0; Lahti and Shetty 2017).

Whole-genome sequencing

Sample selection. Symptomatic leaf homogenate (200 µl) was streaked onto 60-mm lysogeny broth (LB) agar plates (Bertani 1951) containing 25 µg/ml nitrofurantoin and 40 µg/ml cephalexin and incubated at room temperature. When colonies could be observed, each plate was noted for fungal presence and bacterial morphology. *Pseudomonas*-like colonies were then selected from each plate and re-streaked three times to obtain pure culture. If *Pseudomonas*-like morphology was not seen, the predominant colony type was selected. After the third passage, single colonies were inoculated into 2 ml of LB and incubated at room temperature for 2 days with shaking at 200 rpm. Liquid culture (500 µl) was then added to an equal volume of 50% glycerol and frozen at −80°C. One milliliter of the liquid inoculum was also retained for DNA extraction. Seventy microliters of the crude leaf homogenate from both the symptomatic and asymptomatic samples was inoculated into 2 ml of non-selective LB and incubated for 2 days at room temperature with shaking at 200 rpm. After incubation, 500 µl of the liquid culture was stored at −80°C as described previously.

Samples were selected for whole-genome sequencing after the third passage stage described above. As several non-Psa colony phenotypes were observed, isolates were selected to represent a variety of these phenotypes, as well as sampling for representation across regions and host genotypes (Supplementary Table S6).

DNA extraction and sequencing. A Promega Wizard Kit (Promega Corporation, Madison, WI, U.S.A.) was used to extract DNA for whole-genome sequencing. The kit was used according to the manufacturer's instructions, with the exception that 3 µl of RNase was used rather than the recommended 2 µl.

Whole-genome sequencing was performed by Novogene China (https://www.novogene.com) via Auckland Genomics (https://www.auckland.ac.nz/en/science/about-the-faculty/share-shared-research-equipment/auckland-genomics.html). Library preparation was done using a purePlex DNA Library Prep Kit (seqWell, Beverly, MA, U.S.A.). Sequencing was carried out using an Illumina MiSeq 2 × 150-bp PE Nano platform.

Bioinformatic analysis. Whole-genome sequencing reads were assembled using shovill (version 1.1.0; https://github.com/tseemann/shovill), and the resulting contigs were annotated with Prokka (version 1.14.5; Seemann 2014) using the default prokaryotic database. Reference isolates were also annotated with Prokka (Seemann 2014). The phylogeny was built on representative isolates from the *Pseudomonas syringae* species complex phylogroups from Dillon et al. (2019), as well as non-*syringae* representatives from each *Pseudomonas* subgroup. These isolates were used for pangenome analysis with panaroo (version 1.3.0; Tonkin-Hill et al. 2020) to produce an alignment of core genes (panaroo options: --clean-mode strict -a core --remove-invalid-genes --aligner mafft --core_threshold 0.90). A phylogeny was produced from this core gene alignment with RAxML (options -f a -p 12345 -x 12345 -# 100 -m GTRCAT version 8.2.10; Stamatakis 2014). The R package ggtree (Yu et al. 2017) was used to visualize the resulting phylogenies.

Magic-BLAST (version 1.7.2; Boratyn et al. 2019) was used to BLAST custom databases of reference type III secretion systems (T3SSs) and effectors against germplasm isolates. The databases for both effectors and T3SSs were created with sequence data from Dillon et al. (2019) using the magic-BLAST function 'makeblastdb' (options: -dbtype nucl -parse_seqids; Boratyn et al. 2019). The databases were then used to search against the germplasm isolates using the NCBI+ function blastn (Camacho et al. 2009). To validate effector hits, putative effectors were mapped to germplasm isolate genomes manually in Geneious Prime (version 2022.0.1), and the best alignment was selected. For T3SS analysis, homologous regions were extracted from representative genomes to build a custom database (Supplementary Table S7; Araki et al. 2006). The database was then used to search the germplasm isolates to identify the most similar T3SS. Once a candidate T3SS was identified, the individual genes of the corresponding T3SS were mapped to the germplasm isolate genome. Toxins were identified using antiSMASH under relaxed detection strictness (version 7.0; Blin et al. 2023). Results with under 60% similarity were then filtered out. For the Psa3 ICMP 18884 and Pfm ICMP 18803 references, antiSMASH version 8.0 was used (Blin et al. 2025).

In-planta assays

Germplasm-derived isolates were selected from the isolates that underwent whole-genome sequencing. They were selected to represent a range of virulence-associated genomic features present, sampled regions, and taxonomic and phylogenetic diversity, if within the *P. syringae* species complex (Table 1). Psa3 V-13 (ICMP 18884) and Pfm LV-5 (ICMP 18803) were used as controls.

Tissue culture plantlets were used for the inoculation of bacterial isolates. All plantlets originated from Plant & Food Research orchard-sourced spring budwood that had been transferred into tissue culture. *A. arguta* AA07_03 plantlets were sourced from Multiflora (Auckland, New Zealand), who maintain and propagate the tissue culture. *A. melanandra* and *A. polygama* plantlets were propagated in-house at Plant & Food Research's MARC (Auckland, New Zealand). All plantlets were grown in 400-ml lidded plastic pottles on half-strength Murashige and Skoog agar. All pottles contained

TABLE 1
Details of germplasm-derived isolates used in pathogenicity testing with *Pseudomonas syringae* pv. *actinidiae* biovar 3 (Psa3) V-13

Isolate	Closest relative	Proposed phylogroup	Host	Host genotype	Region
HP_001	*P. graminis*	–	*Actinidia arguta*	–	Te Puke
HP_004	*P. cichorii*	11	*A. arguta*	AA04_01	Te Puke
HP_006	*P. syringae*	2	*A. melanandra*	ME02_01	Te Puke
HP_007	*P. syringae*	3	*A. melanandra*	ME02_01	Te Puke
HP_009	*P. protegens*	–	*A. arguta*	AA32_01	Te Puke
HP_013	*P. viridiflava*	7	*A. arguta*	AA04_02	Kerikeri
HP_014	*P. quasicaspiana*	13	*A. polygama*	PC07_01	Kerikeri
HP_015	*P. sivasensis*	–	*A. polygama*	PC02_01	Kerikeri

between 3 and 5 cuttings and were only used once sufficient leaf surface area for harvesting twenty 1-cm leaf discs was observed.

Pathogenicity assays. The pathogenicity of bacterial strains was assessed via in-planta flooding inoculation as per McAtee et al. (2018). Bacterial strains were grown from frozen glycerol stocks on LB plates supplemented with nitrofurantoin and cephalexin. Colonies were then selected and incubated overnight in 5 ml of liquid LB with shaking at 250 rpm at approximately 20°C. After incubation, 2 ml of culture was centrifuged at 5,000 × *g* for 3 min, and the supernatant replaced with 1 ml of 10 mM $MgSO_4$. The resuspended bacterial cultures then acclimated for 1 h at room temperature before the optical density of cells at 600 nm (OD_{600}) was read. Inocula were then diluted in 500 ml of 10 mM $MgSO_4$ to approximately 10^6 CFU/ml ($OD_{600} = 0.005$), and Silwet L-77 (0.0025%; Momentive Performance Materials, Waterford, NY, U.S.A.) was added. Inoculation was carried out by submerging kiwifruit plantlet containers with the bacterial cells in 500 ml of 10 mM $MgSO_4$ for approximately 3 min. After 3 min, the inoculum was decanted, and the plantlet containers were resealed for incubation at 20°C with a 16-/8-h light/dark cycle. The leftover inoculum (50 µl) was plated at 1,000× dilution to validate viability. Competition assays were conducted in the same way, with the exception that cultures were combined in a 1:1 ratio prior to flooding. Co-inoculated isolates were combined at the same final concentrations.

Leaf samples were taken at 7 days postinoculation. Four technical replicates were taken per plantlet, with four 1-cm leaf discs per technical replicate. Competition assays (germplasm isolate + Psa3 V-13) were performed with three biological replicates. Leaf discs were washed in sterile Milli-Q water for 30 s, and each technical replicate of four leaf discs was placed into an Eppendorf Microcentrifuge Safe-Lock tube with three sterile 3.5-mm stainless steel beads and 350 µl of sterile 10 mM $MgSO_4$. Samples were macerated for two rounds of 1 min each with manual dislodgement of any pellets formed between rounds of maceration at top speed in a Storm24 Bullet Blender (Next Advance).

Leaf homogenate was then serially diluted to 10^{-5} and the diluted homogenate plated out on LB agar plates containing 25 µg/ml nitrofurantoin and 40 µg/ml cephalexin. Colonies were then counted at the lowest dilutions possible and used to calculate CFUs/cm^2. DNA was extracted from the leaf homogenate using a QIAGEN DNeasy Plant Mini Kit (QIAGEN), according to the manufacturer's instructions. Extracted DNA was then assessed for bacterial growth using qPCR.

qPCR. Real-time qPCR was used to quantify the results of pathogenicity assays. The primers used for each germplasm isolate are outlined in Supplementary Table S8. Primers were designed against single-copy genes present in the genome of the germplasm isolates that were confirmed to be absent from the Psa3 V-13 genome. The primers were validated against the target isolate using PCR and subsequent gel visualization, as well as against Psa3 V-13 as a negative control to rule out off-target amplification. The primers were further validated using a serial dilution of target isolate DNA to assess primer efficiency, and all were determined to be within the valid range for use (90 to 120% efficiency). The qPCR parameters were based on previous work by Andersen et al. (2018).

Data visualization. Analysis of pathogenicity assay data was performed in R (version 4.2.1; R Core Team 2024). The packages 'tidyverse' (version 2.0.0; Wickham et al. 2019) and 'ggplot2' (version 3.5.1; Wickham 2016) were used for data manipulation and plot creation, respectively. Normality of data was assessed using the Shapiro–Wilk test. For comparisons between individual and co-inoculations, the function stat_compare_means() from the 'ggpubr' package (version 0.6.0; Kassambara 2017) was used. Kruskal–Wallis and Wilcoxon tests were used to analyze statistical differences between groups for nonnormal data; one-way analysis of variance and Welch's *t* test were used to compare normally distributed data. Treatments were pairwise compared with Tukey's honestly significant difference post hoc at 5%, and a compact letter display was used on plots.

Results

P. syringae dominates bacterial communities in symptomatic leaves of diverse *Actinidia* species

In December 2022, symptomatic leaves were sampled from diverse *Actinidia* species in germplasm collections at Plant & Food Research's Kerikeri and Te Puke research orchards (Fig. 1A). Paired samples were taken, with leaf discs sampled from symptomatic lesions and asymptomatic areas of the same leaf (Fig. 1A). Despite widespread observation of leaves with angular, necrotic leaf spots (Supplementary Fig. S1), Psa was isolated from only 24 out of more than 200 symptomatic samples following selective isolation (Fig. 1B; Hemara et al. 2025a). Despite this low frequency of Psa isolation, when using DNA extracted directly from leaf homogenate, all symptomatic samples (bar four) tested positive for the presence of Psa by qPCR (Fig. 1C). In contrast, none of the asymptomatic samples tested positive (Fig. 1C), suggesting that pathogen presence can be spatially limited across samples taken from the same leaf, mere centimeters apart. This low rate of Psa recovery was surprising, especially given the near-ubiquitous presence of Psa in the symptomatic samples. To investigate whether other bacteria could be contributing to symptom development, we sought to characterize the bacterial communities associated with disease symptomatology across the sampled *Actinidia* germplasm.

Thirty-seven paired symptomatic and asymptomatic samples were selected from 16S amplicon sequencing, representing 13 *Actinidia* species that appeared symptomatic in the germplasm. V5 to V9 primers demonstrated to be discriminatory against plant amplicons were chosen to reduce off-target amplification of plastid DNA and to improve the effective sequencing depth (Mayer et al. 2021), and few plastid or mitochondria ASVs were observed (Supplementary Table S5). The total number of sequencing reads per sample is reported, with most samples falling within an acceptable sequencing depth range of 75,000 to 150,000 reads (Supplementary Fig. S2). Amplicon sequencing controls showed the successful taxonomic classification of ONT-derived ASVs (Supplementary Fig. S3). All but six symptomatic samples were dominated by *Pseudomonas*, specifically ASVs that appeared to fall within the Psa/Pth/Pfm clade in phylogroup 1 of *P. syringae* (Fig. 2A). This is in line with qPCR reporting of Psa presence in virtually all symptomatic samples (Fig. 1C). These same ASVs (1, 2, 3, 4, 5, 8, 9, and 12) were present in the Psa3 V-13 gDNA control (Supplementary Fig. S3), suggesting that these ASVs most likely represented Psa3. These ASVs were also present in most asymptomatic samples, albeit at a much lower relative abundance than the corresponding symptomatic samples (Fig. 2A). The Psa/Pth/Pfm ASVs 1 and 2 were some of the most abundant and appeared to be core members of the community across all samples (at a core threshold of 80%). Similarly, the Psa/Pth/Pfm ASVs 1, 2, 3, 4, 5, and 9 were core members of the symptomatic samples. The symptomatic status of samples, which largely corresponds to the presence of this Psa/Pth/Pfm clade, resulted in a statistically significant reduction in the presence of other bacterial genera, as observed in compositional (Fig. 2A) and alpha-diversity plots (Supplementary Fig. S4). Whereas symptomatic status and host species contribute to bacterial diversity, the contribution of region to Shannon diversity was statistically insignificant (Supplementary Figs. S4 and S5; Supplementary Table S9).

Although *Pseudomonas* dominated symptomatic samples, *Sphingomonas* and *Xanthomonas* ASVs were also present across many samples, and *Xanthomonas* was found to be present almost exclusively in symptomatic samples (Fig. 2A). Furthermore, the asymptomatic samples had diverse genera, such as *Sphingomonas*, *Burkholderia*, *Cutibacterium*, *Methylobacterium*, and *Pantoea* (Fig. 2A). ASV7, assigned to *Burkholderia*, was a core member of the community found in asymptomatic samples. Other ASVs of note, which appeared to be differentially abundant in asymptomatic tissue, included *Cutibacterium acnes* (ASVs 13 and 14). Sequencing of our mock community and no-template control indicated that this was not contamination during the extraction and sequencing processes (Supplementary Fig. S3).

When samples were grouped by host, it was apparent that some species had distinct bacterial communities (Fig. 2B). For example, *A. callosa* and *A. chrysantha* symptomatic samples were domi-

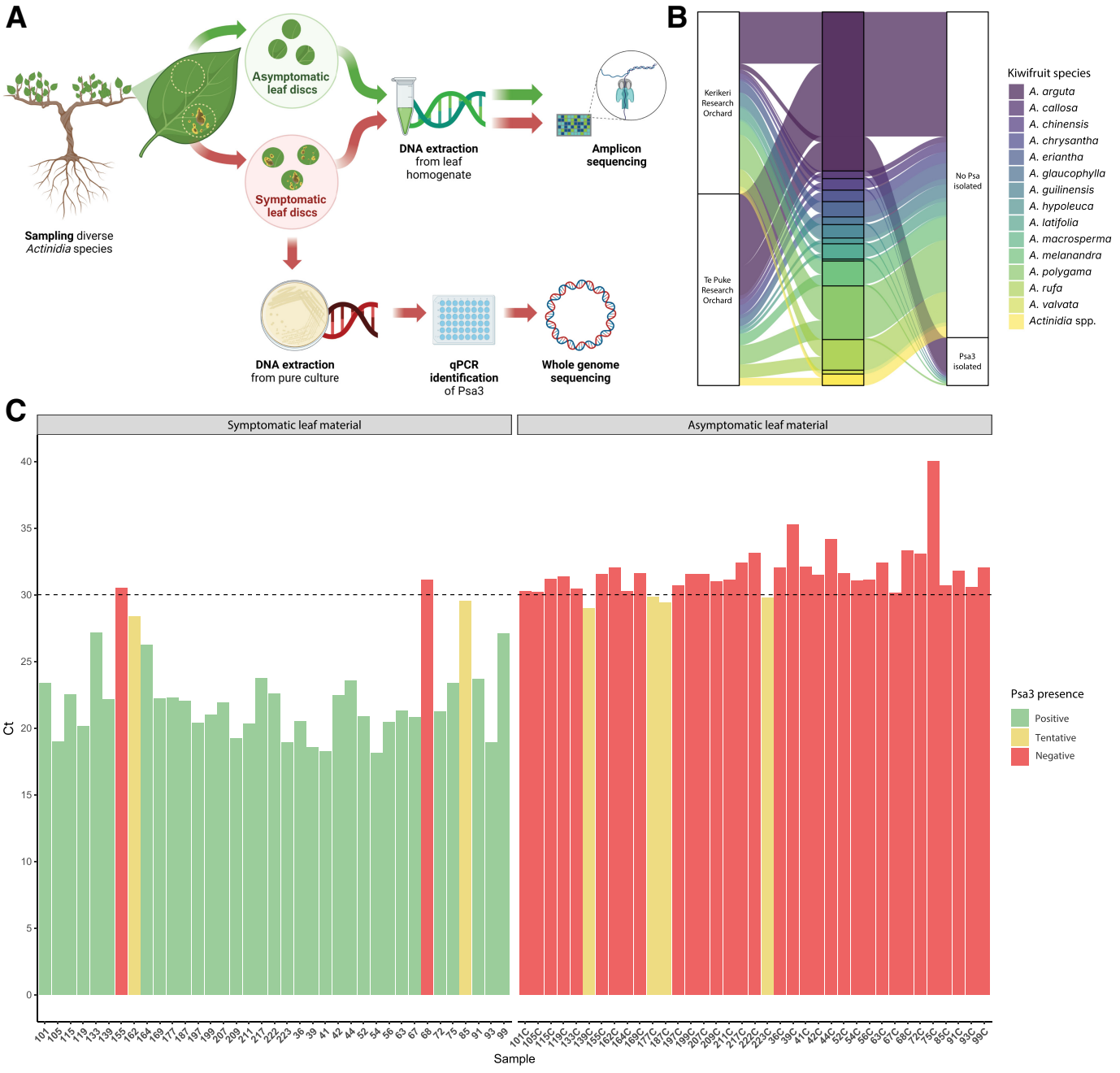

Fig. 1. Low recovery of *Pseudomonas syringae* pv. *actinidiae* (Psa) isolates from symptomatic leaves in the *Actinidia* germplasm. **A,** Germplasm sampling workflow schematic. Symptomatic leaf samples were taken from *Actinidia* germplasm vines. Symptomatic and asymptomatic leaf discs were sampled from each leaf and split into two sample sets. Genomic DNA was extracted from leaf homogenate for quantitative PCR (qPCR) and amplicon sequencing. Leaf homogenate from symptomatic leaf discs was also plated on selective agar for *Pseudomonas* isolation. The resulting pure cultures underwent DNA extraction, qPCR testing for the presence of Psa, and whole-genome sequencing. **B,** Proportion of Psa isolations on selective agar from symptomatic leaf material, as confirmed by qPCR. **C,** Presence of Psa in symptomatic leaf homogenate samples prepared for amplicon sequencing. Presence of Psa was assessed using qPCR with Psa F1/R2 primers (Andersen et al. 2018). Samples are grouped by sample status (symptomatic or asymptomatic). The horizontal dashed line indicates the cycle threshold (Ct) cut-off used to determine Psa presence.

nated by the Psa/Pth/Pfm clade, whereas the corresponding asymptomatic samples were diverse (Fig. 2B). Similar observations can be made for *A. rufa* and *A. latifolia*, albeit to a lesser extent (Fig. 2B). *A. glaucophylla* and *A. guilinensis* communities showed the highest alpha diversity (Supplementary Fig. S5), reflected in high genera diversity and low abundance of Psa/Pth/Pfm (Fig. 2B). Interestingly, the bacterial communities of symptomatic *A. glaucophylla* and *A. guilinensis* samples were similar to those of asymptomatic samples from other hosts, with lower abundance of *Pseudomonas* (Fig. 2B). Notably, *A. guilinensis* symptomatic samples had abundant *Staphylococcus* ASVs (Fig. 2B). Finally, symptomatic *A. glaucophylla*, *A. guilinensis*, and, to a lesser extent, *A. eriantha*, *A. hypoleuca*, and *A. macrosperma*, had relatively less Psa/Pfm/Pth than other species (Fig. 2B).

In select samples from *A. hypoleuca*, *A. melanandra*, *A. arguta*, and *A. polygama*, the Psa/Pfm/Pth clade was observed to co-occur with other *P. syringae* (Fig. 2B). However, these leaves did not appear to differ in symptomology from other representatives of the same *Actinidia* species where only the Psa/Pfm/Pth clade was present (Supplementary Fig. S1). Moreover, germplasm hosts on which we have seen Psa3 effector loss variants emerge, including *A. arguta* and *A. melanandra*, had high abundance of Psa/Pth/Pfm despite their Psa resistance (Fig. 2B; Hemara et al. 2022, 2025a). Previously, when Psa3 effector loss has been observed on germplasm vines, either *avrRpm1a* or *hopAW1a* has been lost, both of which are recognized by *A. arguta* and *A. melanandra* (Hemara et al. 2025a). However, even on resistant vines, effector loss has generally been a rare occurrence across both germplasm and commercial orchard settings (Hemara et al. 2025a, b). This relatively high Psa3 abundance on presumably resistant hosts could be explained if resistance-escaping, effector loss variants have spread in the germplasm. However, only sample 39 from *A. melanandra* yielded an effector loss variant, Psa3 X_477, which has lost *avrRpm1a* (identified through whole-genome sequencing; Hemara et al. 2025a). The limited identification of effector loss variants from this sampling year suggests that the majority of these Psa/Pth/Pfm ASVs are Psa3 lineages carrying the full effector-triggered immunity-eliciting effector repertoire.

Diverse *Pseudomonas* spp. isolated from symptomatic material carry genes belying pathogenic potential

Although ASV analysis revealed dominant genera, species, and (in some instances) specific lineages, partial 16S amplicons do not allow for full taxonomic resolution to the pathovar or biovar level. Despite the dominance of the Psa/Pth/Pfm clade in leaf homogenate samples, diverse *Pseudomonas* were isolated from symptomatic plant material (Fig. 1A). The isolation strategy used in this work indiscriminately captured both epiphytic and endophytic bacteria from symptomatic tissue, making it plausible that some of these isolates could be colonizing the apoplastic space

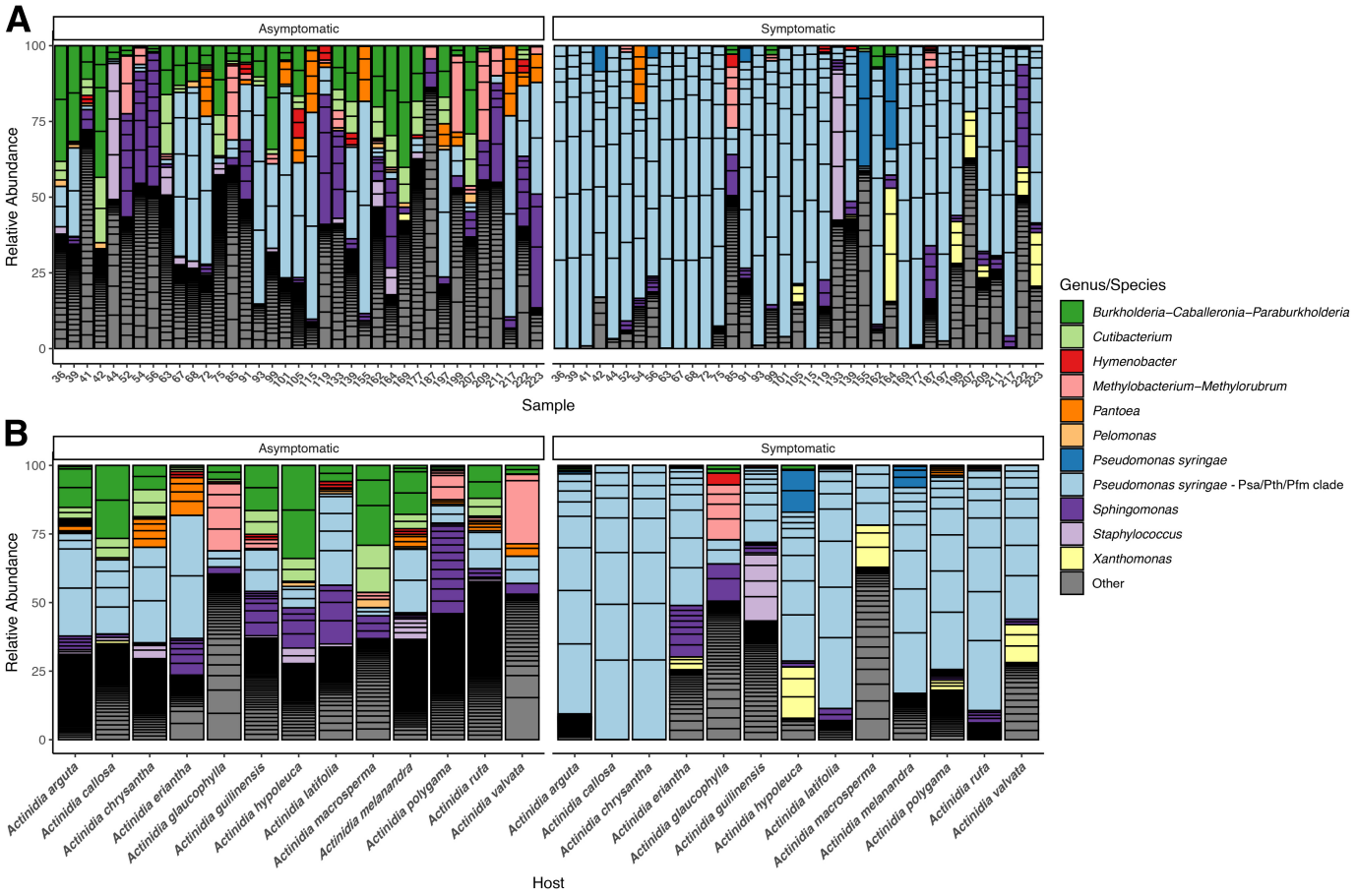

Fig. 2. Dominant bacterial genera present in the *Actinidia* phyllosphere, by symptom status and host species. **A,** Compositional bar plot of *Actinidia* phyllosphere communities by symptom status. The 50 most abundant amplicon sequence variants (ASVs) are represented, colored by genus. **B,** Compositional bar plot of *Actinidia* phyllosphere communities collated by *Actinidia* host. The 50 most abundant ASVs are represented, colored by genus. ASVs identified as "*Pseudomonas syringae* – Psa/Pth/Pfm clade" were identified by BLASTn. All other taxa are indicated by the group "Other." Each black box within the bar indicates a different ASV.

and contributing to disease. Whole-genome sequencing was performed on a subset of these isolates, allowing us to assign more detailed taxonomy through comparison with a core gene alignment of *P. syringae* and plant-associated *Pseudomonas* reference genomes (Supplementary Fig. S6). Of the 16 germplasm isolates analyzed, 12 were categorized within the *P. syringae* species complex: five isolates fell into phylogroup 3, three into phylogroup 2, and one each into phylogroups 7, 11, and 13 (Supplementary Fig. S6). One further isolate, HP_008, remained unassigned to a phylogroup within the *P. syringae* species complex, clustering with PsyCFBP13 (Supplementary Fig. S6). HP_009 fell within the *P. protegens* subgroup, HP_015 within the *P. fluorescens* subgroup, and HP_001 and HP_012 within the *P. lutea* group (Supplementary Fig. S6). Interestingly, when the 16S sequences of these germplasm isolates were compared with our *Pseudomonas* ASVs, these isolates universally appeared to be present only in one or two samples, and at low abundance.

To ascertain the pathogenic potential of these HP germplasm isolates, the isolates' genomes were first screened for key virulence factors, including pathogenicity-associated islands (PAIs) encoding T3SSs for effector delivery, type III secreted effector repertoires, and pathogen-associated secondary metabolite biosynthetic pathways (Xin et al. 2018). As expected, all seven isolates from canonical *P. syringae* phylogroups had a T3SS R-PAI (Fig. 3). In the non-canonical *P. syringae* phylogroups, two further isolates had S-PAIs, and HP_014 carried a PG13 A-PAI (Fig. 3). Outside of the *P. syringae* species complex, some isolates carried T-PAIs (Fig. 3). Overall, only three isolates had no identifiable PAI (Fig. 3). Twenty-five families of effectors were found in the genomes of germplasm isolates (Fig. 3). The most frequent effector family was HopB2, followed by AvrE1. However, across all these genomes, as well as the manually curated Psa3 V-13 assembly, HopB2 lacked an HrpL box. Prior to effector family reassignment (Dillon et al. 2019), HopB2c was previously annotated in the Psa3 V-13 genome as Aconitase A, a core gene in the lipopolysaccharide locus, and may be mischaracterized as an effector. All isolates from canonical *P. syringae* phylogroups carried AvrE1, HopM, HopAA1, and HopI1 (Fig. 3), which have previously been identified as core effectors (Dillon et al. 2019; Lindeberg et al. 2012). Although many isolates carried effectors from the same family, these effectors often belonged to different subtypes (Supplementary Table S10). However, these isolates all carried far fewer effectors than either Psa3 or Pfm, which each encoded over 30 (Fig. 3). HP_006 and HP_011, both from phylogroup 2, carried the highest number of effectors at 13 (Fig. 3). Conversely, non-canonical *P. syringae* HP_014 carried only a single effector (Fig. 3). Non-canonical HP_008 and isolates outside the *P. syringae* species complex did not carry any *P. syringae*-related effectors, despite HP_012 and HP_001 appearing to carry a canonical and alternate T-PAI, respectively (Fig. 3). This potentially indicates a limitation in the ability to detect effectors by homology with distantly related strains (Fig. 3).

The presence of secondary metabolite biosynthetic gene clusters was also assessed. The most common secondary metabolite type across all isolates was non-ribosomal peptide synthetases (NRPSs). From these NRPSs, there were at least 12 biosynthetic gene clusters of interest found across these germplasm isolates, spanning a variety of known toxins (anti-host and antimicrobial), siderophores, and surfactants (Fig. 3). A putative NRPS biosynthetic gene cluster is also present in Psa3 V-13, which is sometimes lost alongside co-located recognized effectors (Fig. 3; Hemara et al. 2022).

Host species influence interactions between *Pseudomonas* isolates and Psa3

Non-Psa pseudomonads appear to be minor components of the phyllosphere community yet possess virulence components that could be contributing to the increased pathogenicity of Psa in normally resistant germplasm. To examine the pathogenic potential of these germplasm-derived pseudomonads, in-planta growth was as-

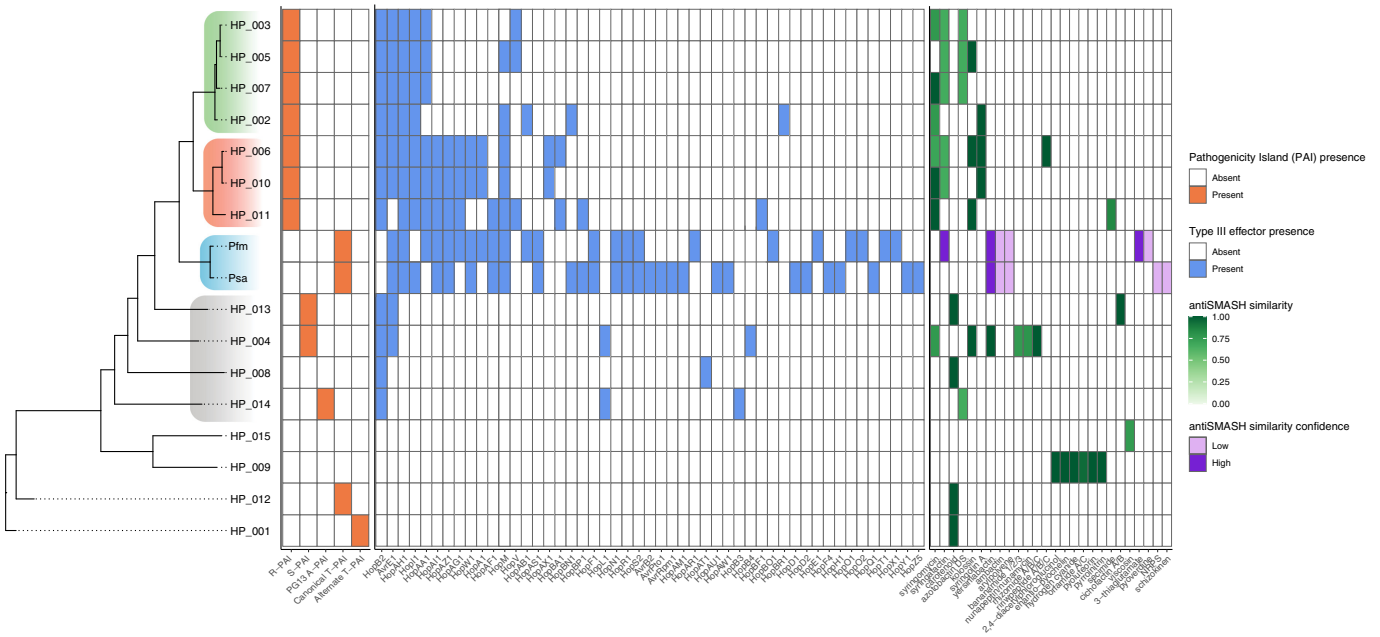

Fig. 3. Pathogenicity-associated traits found across *Pseudomonas* germplasm isolates. Phylogeny colors represent *Pseudomonas syringae* phylogroups 1 (blue), 2 (red), and 3 (green), as well as non-canonical *P. syringae* (gray). Pathogenicity island types expected in the *Pseudomonas syringae* species complex. *P. syringae* effectors, as defined in Dillon et al. (2019), are ordered by prevalence. For germplasm isolates, gene clusters with ≥60% similarity to known secondary metabolites, as identified by antiSMASH (version 7.0; Blin et al. 2023). For *Pseudomonas syringae* pv. *actinidiae* (Psa) and *P. syringae* pv. *actinidifoliorum* (Pfm), similarity confidence is indicated for gene clusters with hits against known secondary metabolites, as identified by antiSMASH (version 8.0; Blin et al. 2025).

sessed across diverse kiwifruit hosts, including *A. arguta* AA07_03, *A. melanandra* ME02_01, and *A. polygama* PC02_01, as well as the susceptible kiwifruit model plant *A. chinensis* var. *chinensis* 'Hort16A'. Hort16A was used to compare plate count and qPCR quantification, validating the use of isolate-specific primers for relative quantification of in-planta growth (Supplementary Fig. S7). Interestingly, HP_013 from phylogroup 7 appeared to grow as well as virulent Psa3 V-13 on this susceptible host (Supplementary Fig. S7). Isolates HP_004, HP_014, HP_001, and HP_007 had comparable growth to the non-pathogenic epiphyte Pfm, infecting Hort16A poorly (Supplementary Fig. S7). The remaining three isolates tested (HP_015, HP_009, and HP_006) showed intermediate infection of Hort16A (Supplementary Fig. S7).

On the germplasm hosts *A. arguta*, *A. melanandra*, and *A. polygama*, these isolates appeared to have relatively lower bacterial growth than on susceptible Hort16A (Fig. 4; Supplementary Fig. S7). The majority of these isolates were non-pathogenic in single-isolate infections, with pathogenicity defined as the qualitative ability to infect and cause symptoms on a host (Sacristán and García-Arenal 2008). Furthermore, it appears that isolates do not have any "home advantage" on the host they were isolated from (Fig. 4). On *A. arguta*, only a few isolates had significantly different growth from that of recognized (i.e., avirulent) Psa3 V-13 (Fig. 4A). HP_004 was significantly different from Psa3 V-13, with slightly higher in-planta growth, and HP_014 demonstrated the poorest growth by a large margin (Fig. 4A). On *A. melanandra*, germplasm isolates were more similar to one another: isolates HP_006, HP_001, and HP_015 had reduced growth compared with the recognized Psa3 V-13, with all other isolates not significantly different from this control (Fig. 4B). Finally, on *A. polygama*, all isolates demonstrated relatively

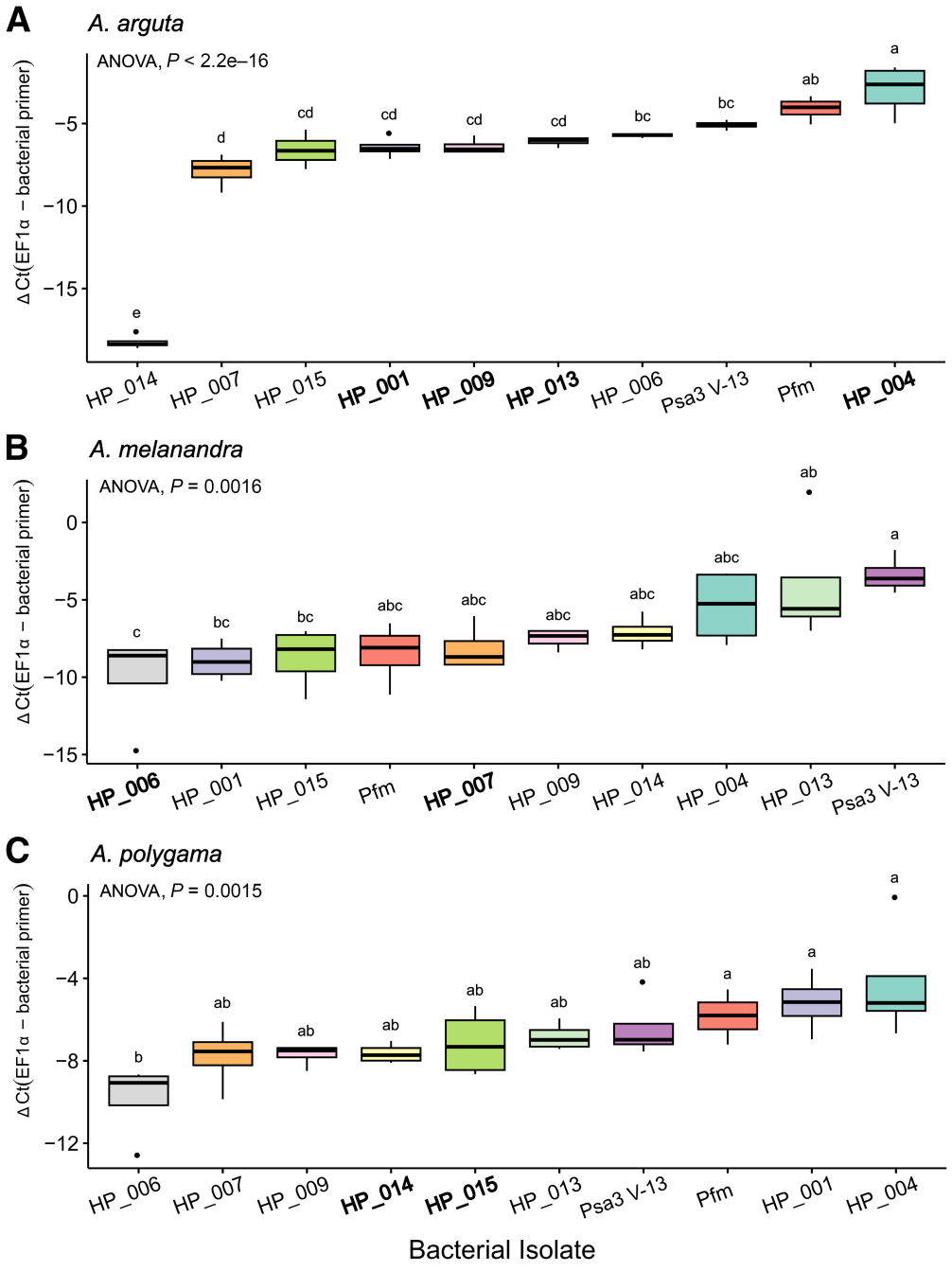

Fig. 4. Results of quantitative PCR analysis of bacterial growth of germplasm isolates in three species of *Actinidia* plantlets at 7 days postinoculation. Plantlets were flooded with 10^6 CFU/ml of each bacterial isolate. Bacterial growth was quantified by quantitative real-time qPCR using isolate-specific primers and normalizing the cycle threshold (Ct) to a plant housekeeping gene, EF1α, to get a ΔCt value. The isolates were tested against **A,** *Actinidia arguta*; **B,** *Actinidia melanandra*; and **C,** *Actinidia polygama* plantlets. The isolates highlighted with bold font on the *x* axis were isolated from that respective species. Black bars represent the median values, and box whiskers indicate total range of four technical replicates. The compact letter display above each box indicates significant differences between bacterial isolates using Tukey's honestly significant difference post-hoc test at 5%.

low growth, and most were not significantly different from one another (Fig. 4C). Across all germplasm hosts, none of the isolates, or the controls, showed pathogen-associated levels of growth (Fig. 4). Curiously, however, a distinct leaf collapse and tissue necrosis phenotype was observed when Hort16A, *A. arguta*, and *A. melanandra* (but not *A. polygama*) were infected with HP_013 (Supplementary Fig. S8).

These germplasm isolates remain curious; although not particularly abundant in amplicon sequencing data, these *Pseudomonas* spp. were isolated from symptomatic material from which we expected to recover Psa. Although they have some pathogenic potential, as suggested by their genomic characteristics, the vast majority did not have increased in-planta growth compared with avirulent Psa3 V-13 or epiphytic Pfm on Psa-resistant germplasm species. The lack of independent colonization by these isolates raises the possibility that they may only be opportunistically present in detectable/recoverable quantities during Psa-mediated infection, forming a commensal syndemic interaction (hypothesis 1). Alternatively, because of the low incidence of Psa infection per se in these genotypes, these strains may be facilitating the growth of Psa through formation of syndemic infections, as suspected in previous mixed infections (hypothesis 2) (Purahong et al. 2018; Sadhukhan et al. 2024). To test the potential for either of these dynamics between these germplasm-derived pseudomonads and Psa, 1:1 mixed communities were made for co-inoculation of the *Actinidia* species from which these *Pseudomonas* isolates were derived. On *A. melanandra*, co-inoculation did not have a strong effect on the growth of either the germplasm isolates or Psa3 V-13 (Fig. 5). Compared with individual inoculation, there was no difference in growth when HP_006 and Psa3 V-13 were co-inoculated (Fig. 5A). HP_007 decreased the growth of Psa3 V-13 when co-inoculated ($P = 0.0022$), but its own growth was unaffected when co-inoculated (Fig. 5B). Similar dynamics were observed when Psa3 V-13 was co-inoculated with the control Pfm ($P = 0.033$; Fig. 5C). Curiously, the inverse was observed when isolates HP_014 and HP_015 were tested on *A. polygama* (Fig. 6). On *A. polygama*, the co-inoculation of HP_014 and Psa3 V-13 resulted in the increased growth of both isolates compared with individual inoculation, suggesting syndemic growth of Psa and HP_014 ($P = 0.00051$ and $P = 0.01$, respectively; Fig. 6A). When co-inoculated with HP_015, the growth of Psa3 V-13 also increased ($P = 0.039$), although HP_015 remained unaffected (Fig. 6B). Neither Pfm nor Psa3 V-13 was affected when co-inoculated into *A. polygama*, suggesting that host genotype may influence this syndemic interaction outcome (Fig. 6C; Supplementary Table S11).

Notably, four isolates were derived from *A. arguta*, and co-infections revealed several to have increased growth when co-inoculated with Psa3 V-13 (Fig. 7). Interestingly, *A. arguta* was the only host to exhibit disease symptoms across any of the co-inoculation experiments, with HP_004 and HP_013 co-inoculations greatly increasing the in-planta growth of both Psa3 V-13 and the focal germplasm isolate (Fig. 7B and D). Curiously, this same increase was also observed for Pfm (Fig. 7E), which was not observed on *A. melanandra* (Fig. 5C) or *A. polygama* (Fig. 6C), again highlighting the host specificity of syndemic associations. Only co-inoculation with HP_001 saw no change for either isolate during co-inoculation (Fig. 7A), whereas HP_009 slightly decreased the growth of Psa3 V-13 when co-inoculated (Fig. 7C). Fittingly, these plants appeared asymptomatic following co-inoculation.

Discussion

The aim of this work was to understand the basis of disease symptomatology arising on Psa-resistant *Actinidia* germplasm. Despite the prevalence of Psa3 identified through qPCR and amplicon sequencing, recovery of Psa isolates was low. This poor recovery during culturing could be explained by the fact that Psa grows more slowly than other *Pseudomonas* lineages on agar, taking 30 to 48 h for colonies to appear following room temperature incubation (Tyson et al. 2018). Furthermore, genome biosurveillance found that resistance-breaking Psa3 effector loss isolates are rare (Hemara et al. 2025a). Accordingly, the spread of resistance-breaking Psa3 cannot explain the full extent of symptomatic vines observed. To this end, we characterized the bacterial phyllosphere communities associated with symptomatic and asymptomatic leaf regions. Unsurprisingly, amplicon sequencing demonstrated that Psa infection affects the composition and diversity of bacterial communities, consistent with previous observations in the kiwifruit phyllosphere (Ares et al. 2021; Purahong et al. 2018). Symptomatic samples were dominated by *P. syringae* from the Psa/Pth/Pfm clade, which we assume to represent Psa3. The *Pseudomonas* genus, when present, was almost entirely dominated by this *P. syringae* phylogroup 1 clade. It remains unclear to us why so little Psa3 was isolated from these samples in light of this. Interestingly, there was little detection of other *Pseudomonas* spp. known to be present in New Zealand kiwifruit orchards, such as *P. syringae* phylogroup 3a isolates, which have been found epiphytically on kiwifruit (Straub et al. 2018; Visnovsky et al. 2019). The same holds true for Pss and *P. viridiflava*, which were previously found in *A. chinensis* var. *chinensis* and *A. chinensis* var. *deliciosa* infected with Psa (Purahong et al. 2018). Beyond *Pseudomonas*, *Xanthomonas* ASVs were present almost exclusively in symptomatic samples. Xanthomonads are known to opportunistically form pathogen complexes with *Pseudomonas* in disease settings, such as with *P. syringae* in pepper and tomato infections (Gitaitis et al. 1987). The near-exclusive occurrence of *Xanthomonas* in symptomatic samples could suggest that they have a role in disease or take advantage of Psa's presence to opportunistically co-colonize leaf tissue. Overall, the ability of pathogens to manipulate their host ultimately affects microbial competition and resource availability, likely affecting microbial diversity through both resource utilization and effector-mediated modification of the host's metabolome (Cai et al. 2023; Schlechter et al. 2023).

Certain *Actinidia* species, including *A. glaucophylla* and *A. guilinensis*, are exceptions to the dominance of *Pseudomonas*, harboring diverse communities across both symptomatic and asymptomatic samples. It could be that these species have hyper-resistance against Psa, thus suppressing *Pseudomonas* abundance, as observed at the genus level. Alternatively, differences in *Pseudomonas* abundance across hosts could be attributed to the specific variants present. However, we do not observe this same phenomenon in other *Actinidia* species we know to have strong effector-triggered immunity against Psa3, such as *A. arguta* and *A. melanandra* (Hemara et al. 2022, 2025a). Further still, these studies have highlighted the emergence of effector loss isolates that partially escape host immunity and have improved in-planta growth (Hemara et al. 2022, 2025a). Whether the Psa population present on particular hosts represents "wild-type" Psa3 or effector loss variants could further explain why this Psa/Pth/Pfm clade is dominant on some hosts and not others. However, isolation efforts suggest that effector loss variants were not widespread within this sample set (Hemara et al. 2025a). Other factors are likely at play as well; for example, phyllosphere bacterial communities in *A. chinensis* var. *chinensis* and *A. chinensis* var. *deliciosa* were also influenced by stochastic assembly processes, particularly drift and dispersal (Louisson et al. 2023). In the future, increasing the number of vines sampled and taking advantage of identical accessions planted out in different locations (e.g., New Zealand's *Actinidia* germplasm collections in Kerikeri, Te Puke, and Motueka) will allow us to better understand the

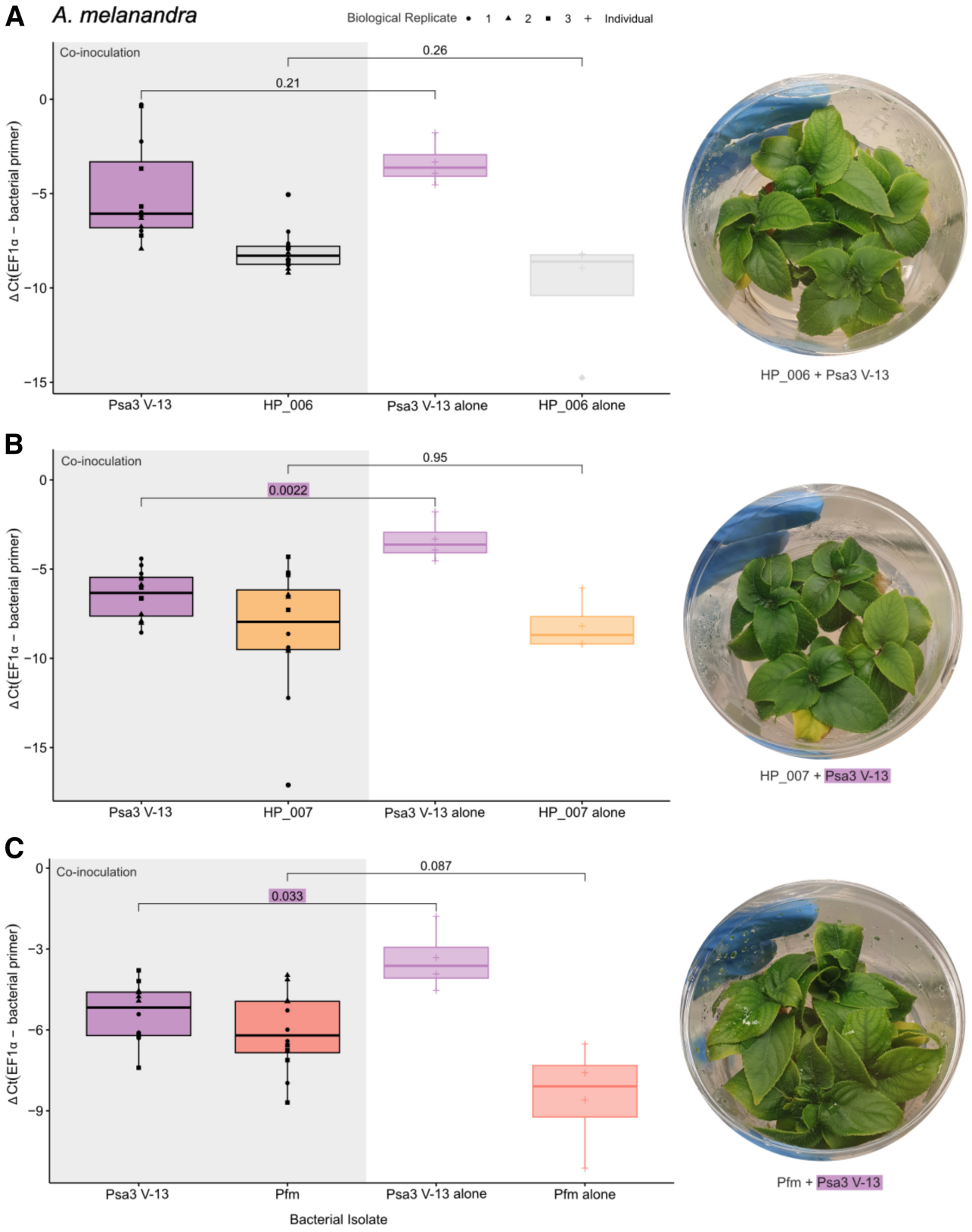

Fig. 5. Results of quantitative PCR analysis of the virulence of germplasm isolates with *Pseudomonas syringae* pv. *actinidiae* (Psa) on *Actinidia melanandra* at 7 days postinoculation (dpi). Plantlets were flooded with 10^6 CFU/ml of bacterial isolates together. Bacterial growth was quantified by quantitative real-time qPCR using isolate-specific primers and normalizing the cycle threshold (Ct) to a plant housekeeping gene, EF1α, to get a ΔCt value. **A,** HP_006 and Psa3 V-13 (*P* value generated with Wilcoxon's test); **B,** HP_007 and Psa3 V-13 (*P* value generated with Wilcoxon's test); and **C,** *Pseudomonas syringae* pv. *actinidifoliorum* (Pfm) and Psa3 V-13 (*P* value generated with Welch's *t* test). Each pane compares the results of the in-planta competition assay with each isolate in the same host alone using a pairwise significance test. Representative plantlet images at 7 dpi are displayed next to the relevant assay. Significant results are highlighted with the color of the variable to which they pertain.

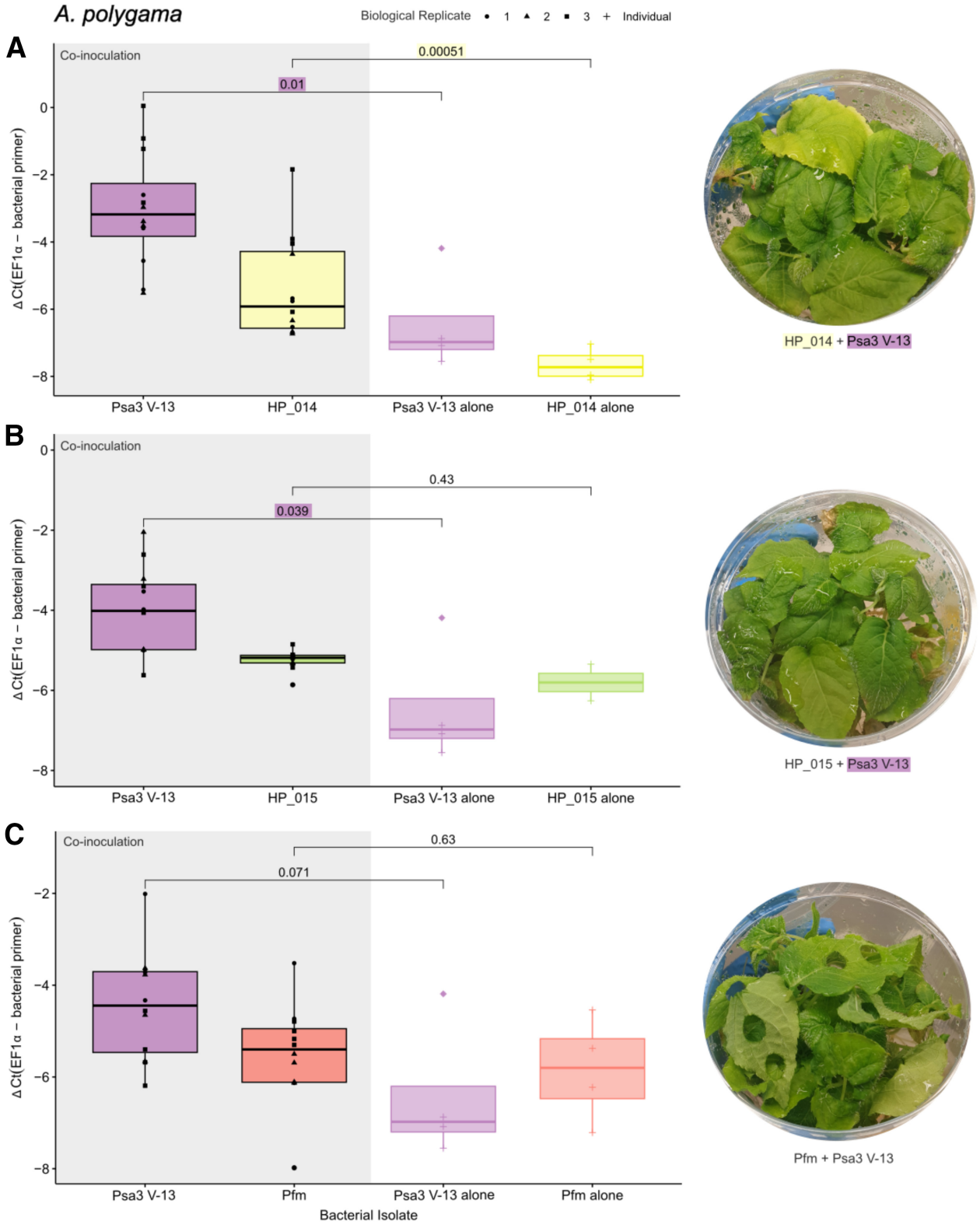

Fig. 6. Results of quantitative PCR analysis of the virulence of germplasm isolates in competition with *Pseudomonas syringae* pv. *actinidiae* (Psa) on *Actinidia polygama* at 7 days postinoculation (dpi). Plantlets were flooded with 10^6 CFU/ml of each bacterial isolate. Bacterial growth was quantified by quantitative real-time qPCR using isolate-specific primers and normalizing the cycle threshold (Ct) to a plant housekeeping gene, EF1α, to get a ΔCt value. **A,** HP-014 and Psa3 V-13; **B,** HP_015 and Psa3 V-13; and **C,** *Pseudomonas syringae* pv. *actinidifoliorum* (Pfm) and Psa3 V-13. Each pane compares the results of the in-planta co-inoculation assay with each isolate in the same host alone, with *P* values generated using Welch's *t* test. Representative plantlet images at 7 dpi are displayed next to the relevant assay. Significant results are highlighted with the color of the variable to which they pertain.

contributions of host genotype, pathogen presence, and stochastic assembly to microbiome composition.

Given the dominance of *Pseudomonas* in symptomatic samples, it is perhaps unsurprising that the most diverse communities were instead observed in asymptomatic leaf tissue. Although the Psa/Pth/Pfm lineage was often present (possibly indicating latent or emerging infections), asymptomatic samples were dominated by *Cutibacterium*, *Sphingomonas*, *Burkholderia*, *Methylobacterium*, and *Pantoea*. Many of these taxa have been implicated in plant protection. For instance, in *P. syringae*-infected tobacco, treatment with biological control agents resulted in greater presence of *Sphingomonas* and *Methylobacterium*, which are suggested to have plant-protective traits through competition and defense priming, respectively (Yang et al. 2024). This aligns with recent work demonstrating that the early recruitment of eubiotic microbiota aids in the development of plant immune responses against pathogens in *Arabidopsis*, without which the plant becomes susceptible to disease (Paasch et al. 2023). However, although the phyllosphere microbiome can sometimes change to benefit the plant after pathogen invasion, reducing dysbiosis and disease severity (Ehau-Taumaunu and Hockett 2023), pathogen perturbation of the phyllosphere through mechanisms such as type VI secretion system-mediated killing can itself lead to dysbiosis (Chen et al. 2020; Smith et al. 2020). More broadly, our focus on pathogen resistance risks overlooking the other beneficial contributions the phyllosphere microbiome may offer, including phytohormone production, nitrogen fixation, and the solubilization of key nutrients (Bashir et al. 2022). The role of phyllosphere bacteria in plant health cannot be downplayed, as they represent a large source of functional diversity for their plant hosts.

Plant genotype is another important contributor to microbiome composition (Bashir et al. 2022; Kusstatscher et al. 2020; Wagner et al. 2020). In this work, host genotype was found to be a significant factor, in line with previous studies in commercial monoculture settings that have shown different varieties to have significantly different microbiome compositions (Louisson et al. 2023; Purahong et al. 2018). Psa-susceptible *A. chinensis* var. *chinensis* previously exhibited higher diversity than Psa-tolerant *A. chinensis* var. *deliciosa*, with *Pseudomonas* spp. 13 times more abundant on var. *deliciosa* than on var. *chinensis* (Purahong et al. 2018). Further still, differences in the phyllosphere microbiomes of these two kiwifruit varieties were more pronounced when a pathogen was present (Purahong et al. 2018). Pathogen-infected *A. chinensis* var. *deliciosa* microbiomes were dominated by over 75% *Pseudomonas* spp., compared with less than 25% in infected *A. chinensis*

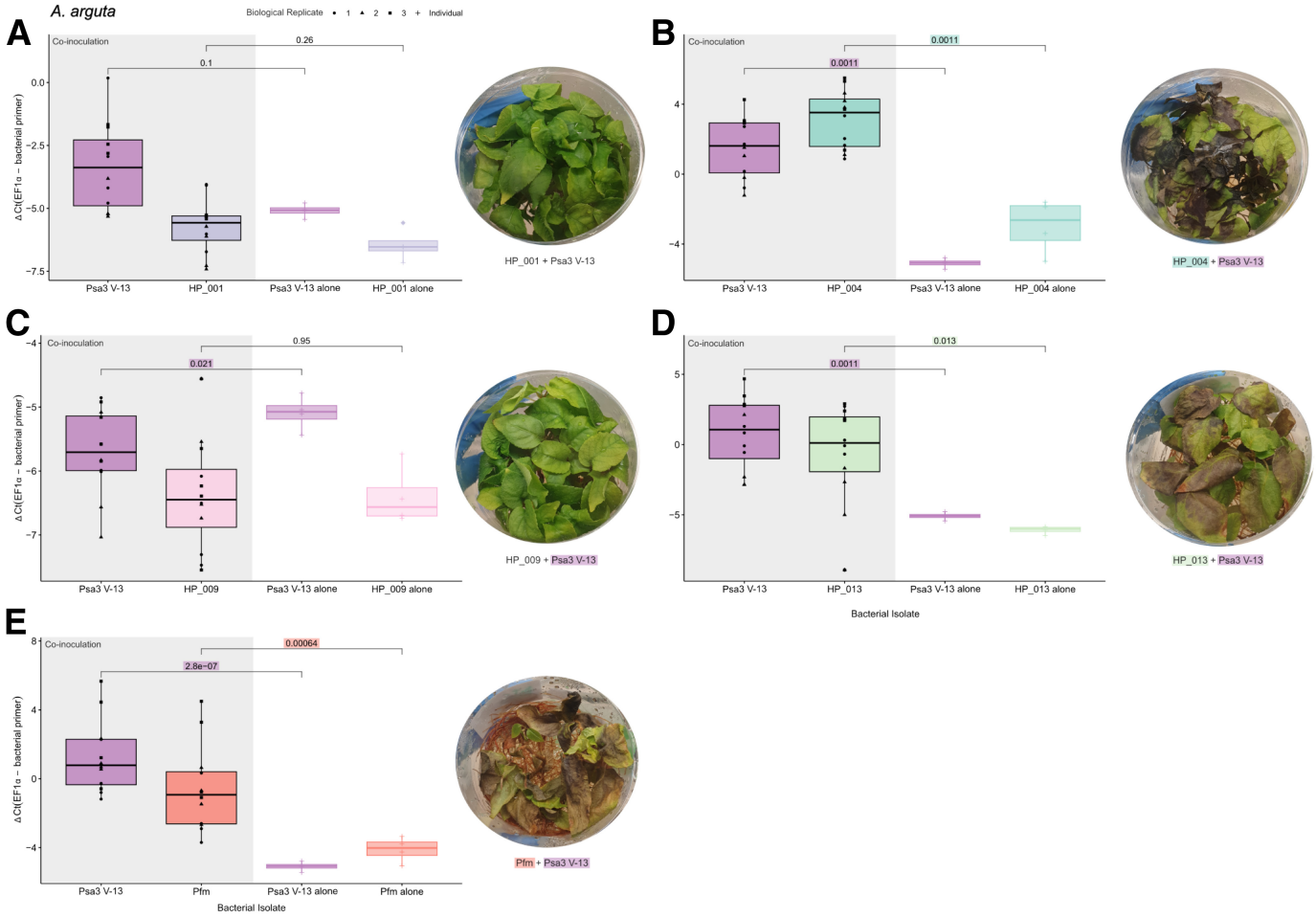

Fig. 7. Results of real-time qPCR analysis of the virulence of germplasm isolates in competition with *Pseudomonas syringae* pv. *actinidiae* (Psa) on *Actinidia arguta* at 7 days postinoculation (dpi). Plantlets were flooded with 10^6 CFU/ml of each bacterial isolate. Bacterial growth was quantified by real-time qPCR using isolate-specific primers and normalizing the cycle threshold (Ct) to a plant housekeeping gene, EF1α, to get a ΔCt value. **A,** HP_001; **B,** HP_004; **C,** HP_009; **D,** HP_013; and **E,** *Pseudomonas syringae* pv. *actinidifoliorum* (Pfm). Each pane compares the results of the in-planta co-inoculation assay with each isolate in the same host alone, with *P* values generated using Welch's *t* test. Representative plantlet images at 7 dpi are displayed next to the relevant assay. Significant results are highlighted with the color of the variable to which they pertain.

var. *chinensis* (Purahong et al. 2018). This suggests that pathogen presence affects the phyllosphere microbiome in a host-dependent manner, which supports similar observations in this work. Differences in the microbiome were attributed to trichome distribution and structure between the two species (Purahong et al. 2018). Based on the phenotypic differences observed in leaves from diverse *Actinidia* spp., it is plausible that a similar phenomenon could be at play in the germplasm. In the tomato phyllosphere, trichomes form genotype-specific microbial hotspots, boosting bacterial diversity when present, particularly *Sphingomonadaceae* and *Burkholderiaceae* (Kusstatscher et al. 2020). Furthermore, it has recently been demonstrated that *Erwinia amylovora* enters apple leaf tissue through natural wounds produced by trichome abscission, which provides another possible explanation as to how trichomes may influence phyllosphere communities (Millett et al. 2025). Several factors affecting the plant-associated microbiota remain to be explored for diverse genotypes in *Actinidia*. Seasonality is a trait that, in conjunction with host genetics, determines microbiome composition (Ares et al. 2021; Howe et al. 2023). Taken together, these works highlight the important influence plant architecture and micro-niches, plant genetics, co-local geographic distribution of hosts, and seasonality may have on community composition.

Whole-genome sequencing of *Pseudomonas* isolates revealed the presence of potential pathogen-associated genomic features, including well-characterized T3SS effectors and several secondary metabolites with potential toxin functions. The presence of PAIs, effectors, phytotoxins, and other secondary metabolites suggests that many of these isolates have pathogenic potential and could contribute to disease observed in the kiwifruit germplasm, especially if they are acting collaboratively with pathogens such as Psa. The diverse secondary metabolite profiles of these isolates are of particular interest: they may aid Psa in its infection process, as local Psa3 isolates possess only a putative NRPS biosynthetic gene cluster, unlike other Psa biovars that carry toxins such as coronatine and phaseolotoxin (Fujikawa and Sawada 2019; Sawada and Fujikawa 2019). In comparison, the effector repertoires of germplasm isolates were generally small compared with Psa and Pfm. This could suggest that these isolates are epiphytic and nonpathogenic, or they may contribute to symptomatology through other means, such as toxins. The widespread presence of AvrE1 suggests a common basic ability among these isolates from symptomatic tissues to induce apoplastic wetting (Nomura et al. 2023). Isolates such as *P. viridiflava* HP_013, which only encodes AvrE1, may not be able to gain entry to the apoplast or suppress plant immunity alone, thus making a partnership with Psa3 V-13 beneficial. However, Psa3 V-13 is recognized on these *Actinidia* species (Hemara et al. 2022, 2025a), implying that isolates with limited individual potential must also be providing colonization or immune suppression advantages to improve in-planta growth outcomes for both isolates when co-inoculated.

Co-inoculation results suggest that some *Pseudomonas* species may be able to form pathogenic complexes in the *Actinidia* phyllosphere, aiding each other to increase proliferation. Individually, Psa alone was unable to cause symptoms on resistant germplasm hosts, and the germplasm isolates were non-pathogenic on *A. arguta*, *A. polygama*, and *A. melanandra* hosts. However, when co-inoculated, several demonstrated a synergistic effect. This outcome is highly host-dependent, which is unsurprising, given that host compatibility is a central part of pathogen success (Sacristán and García-Arenal 2008). The host-specific nature of these interaction outcomes is exemplified by the Pfm control. Notably, Pfm has all the makings of a successful pathogen, including a T3SS and large effector repertoire, yet it is unable to infect both susceptible and resistant hosts alike (Jayaraman et al. 2023). When co-inoculated with Psa3 V-13, Pfm exhibited mutualistic pathogenicity in *A. arguta* yet suppressed Psa3 V-13 growth in *A. melanandra*, with no change in growth observed on *A. polygama*. Many factors may affect this compatibility, including effector and toxin repertoires, T3SS presence and type, and host immune responses. Pathogenic complexes, where consortia form and result in increased disease severity, have previously been demonstrated in *Pseudomonas*. For example, *Xanthomonas perforans* was shown to exhibit higher disease severity in co-infection with both *X. arboricola* and *P. capsici* (Sadhukhan et al. 2024). Consortia formation has also been observed between *P. savastanoi* pv. *savastanoi*, *Pantoea agglomerans*, and *Erwinia toletana* (Hosni et al. 2011). *P. agglomerans* is particularly interesting in that it can both suppress and aid in *P. savastanoi* pv. *savastanoi* knot formation (Hosni et al. 2011). Cooperative virulence through public goods sharing was also recently demonstrated using a *P. syringae* pv. *tomato* metaclone, in which each co-isogenic strain in the community carried only a single effector and was avirulent in isolation but virulent together (Ruiz-Bedoya et al. 2023). This cooperative virulence could also benefit the in-planta growth of other species, such as *P. fluorescens* (Ruiz-Bedoya et al. 2023). This further suggests that pathogenic species can confer virulence benefits to unrelated, nonvirulent members of the phyllosphere. These results suggest that commensal bacteria are flexible in their interactions with pathogens, neatly exemplifying the breadth of the symbiosis spectrum. Our findings add to a growing body of research showing that bacteria can cause disease socially, often with greater severity (Sadhukhan et al. 2024). Such pathogenic consortia may have significant consequences for the epidemiology and subsequent control of resulting incursions, as complex multispecies diseases are inherently more difficult to diagnose and manage (Lamichhane and Venturi 2015).

Conversely, other isolates reduced the growth of Psa in planta. Suppressive microbiomes have been demonstrated in a number of systems. For example, closely related commensal *Pseudomonas* have been demonstrated to suppress pathogenic *Pseudomonas* (Wang et al. 2022). Ehau-Taumaunu and Hockett (2022) demonstrated that Pss populations gain a bacteriocin-mediated in-planta growth benefit when co-infiltrated with the bacteriocin-sensitive *P. syringae* pv. *phaseolicola*, which appears to be dependent on effector-mediated virulence. This again highlights that pathogen proliferation relies on suppression of host defense responses and forms the background against which microbe–microbe interactions take place. Disease-suppressive phyllosphere communities have also been successfully developed through serial passaging, reducing disease severity in tomato infected with *P. syringae* pv. *tomato* DC3000 (Ehau-Taumaunu and Hockett 2023).

It is worth noting, in the context of this research, that the ratio at which these germplasm isolates were co-inoculated is not reflective of the abundance of these isolates in the field. Straub et al. (2018) performed competitive growth assays with Psa3 NZ54 and the *P. syringae* phylogroup 3a isolate G33C at both a 1:1 ratio and a "rare" invasion ratio of 1:100 on *A. chinensis* var. *chinensis* varieties, which may better capture field population structures. Co-inoculation reduced the epiphytic and endophytic growth of Psa in early growth stages, in a variety-specific manner (Straub et al. 2018). On the other hand, co-inoculation increased the growth of *P. syringae* G33C, even when co-inoculated with a T3SS-lacking Psa3 Δ*hrcC* mutant that cannot secrete effectors, suggesting that this benefit cannot be attributed solely to Psa's effector-mediated virulence (Straub et al. 2018). The effects of population density on colonization, resource competition, antimicrobial compound and phytotoxin accumulation, contact-dependent growth inhibition, and bacteriocin action must be considered (Straub et al. 2018). Future

work should endeavor to build synthetic communities that better represent in-field dynamics—in membership, structure, and inoculation method.

The combined or collective pathogenicity of isolates in the *Actinidia* phyllosphere does not necessarily depend on the virulence-associated features, such as effectors and phytotoxins, of the co-infecting partner. There did not appear to be any strong correlations between virulence-associated factors and observed pathogenicity in this work. On the contrary, we have demonstrated that commensal or weakly pathogenic bacteria can move across the spectrum of symbiosis and contribute to disease, similarly to interactions between *Pseudomonas* spp. observed in *Phaseolus vulgaris* (Rufián et al. 2018). Isolates with small effector and toxin repertoires significantly increased in-planta growth during co-inoculation, whereas isolates such as HP_006 with relatively larger repertoires had no effect on Psa growth in planta. Strains in *P. syringae* phylogroup 2 are thought to possess fewer effectors than other phylogroups while maintaining conserved toxin pathways, possibly making them better epiphytes than other phylogroups (Grenz et al. 2025; Vadillo-Dieguez et al. 2024) It is possible that these smaller repertoires allow these isolates to manage the burden of Psa's recognition, allowing for proliferation of both the isolate and Psa3 V-13. The results of this work, particularly the possible formation of pathogen complexes, are concerning. However, this work demonstrates a range of interaction outcomes, with other isolates showing the potential to reduce Psa's growth. Further testing is needed to determine how isolates might interact in more complex community assemblages in planta. Future work should also explore extending this view of microbial interplay, to capture fungi and other eukaryotic microbes present in the phyllosphere.

Finally, recent advances in metagenomics could help us understand the prevalence of species, lineages, and variants in the disease-associated phyllosphere (Benoit et al. 2024; Bickhart et al. 2022; Burton et al. 2014; Marbouty et al. 2014). Metagenome-assembled genomes may allow for less-biased detection of potential and emerging pathogens, given the labor-intensive nature of traditional isolation-based genome biosurveillance. Further still, metagenomics offers a powerful lens to improve our understanding of phyllosphere communities, allowing us to identify and track effector repertoires across all members, providing insights into the potential for the emergence of virulence or cooperative phenotypes. Alternatively, this could also be achieved through targeted amplicon sequencing of genes of interest, particularly effectors and known toxins. This approach has recently been demonstrated by Byers et al. (2024), who surveyed the diversity of secondary metabolite biosynthetic gene clusters in kauri forest soils. By characterizing the genomic potential of these communities, we can better understand the broader context in which known pathogens such as Psa exist and from which both new pathogens and new biocontrol agents may emerge. The research presented here provides a foundation for future studies aimed at elucidating the mechanisms of cooperative virulence and disease suppression in the phyllosphere, helping to protect crops against emerging threats, potentially through the development of new disease management strategies and agents.

Acknowledgments

The authors thank Sidney Scott for assistance with germplasm sampling; Juanita Dunn and Gavin Lloyd for assistance with research orchard access; Hanareia Ehau-Taumaunu, Virginia Marroni, and Hayley Ridgway for manuscript review; and Nikki Freed and the team at Auckland Genomics for DNA sequencing support. The authors also acknowledge the use of New Zealand eScience Infrastructure (NeSI) high-performance computing facilities, consulting support, and training services as part of this research. New Zealand's national facilities are provided by NeSI and funded jointly by NeSI's collaborator institutions and through the Ministry of Business, Innovation & Employment's Research Infrastructure program (https://www.nesi.org.nz).

Literature Cited

Andersen, M. T., Templeton, M. D., Rees-George, J., Vanneste, J. L., Cornish, D. A., Yu, J., Cui, W., Braggins, T. J., Babu, K., Mackay, J. F., and Rikkerink, E. H. A. 2018. Highly specific assays to detect isolates of *Pseudomonas syringae* pv. *actinidiae* biovar 3 and *Pseudomonas syringae* pv. *actinidifoliorum* directly from plant material. Plant Pathol. 67:1220-1230.

Andrews, S., Krueger, F., Segonds-Pichon, A., Biggins, L., Krueger, C., and Wingett, S. 2010. FastQC: A quality control tool for high throughput sequence data. http://www.bioinformatics.babraham.ac.uk/projects/fastqc

Araki, H., Tian, D., Goss, E. M., Jakob, K., Halldorsdottir, S. S., Kreitman, M., and Bergelson, J. 2006. Presence/absence polymorphism for alternative pathogenicity islands in *Pseudomonas viridiflava*, a pathogen of *Arabidopsis*. Proc. Natl. Acad. Sci. U.S.A. 103:5887-5892.

Ares, A., Pereira, J., Garcia, E., Costa, J., and Tiago, I. 2021. The leaf bacterial microbiota of female and male kiwifruit plants in distinct seasons: Assessing the impact of *Pseudomonas syringae* pv. *actinidiae*. Phytobiomes J. 5:275-287.

Asif, M., Hu, R., Xie, T., Fan, R., Long, Y., Wang, Y., Wu, S., Zhao, Z., and Huang, L. 2025. Novel insights into the genetic basis and transcriptomic elucidation of virulence attenuation in *Pseudomonas syringae* pv. *actinidiae* variants. Virulence 16:2543983.

Bashir, I., War, A. F., Rafiq, I., Reshi, Z. A., Rashid, I., and Shouche, Y. S. 2022. Phyllosphere microbiome: Diversity and functions. Microbiol. Res. 254:126888.

Benoit, G., Raguideau, S., James, R., Phillippy, A. M., Chikhi, R., and Quince, C. 2024. High-quality metagenome assembly from long accurate reads with metaMDBG. Nat. Biotechnol. 42:1378-1383.

Bertani, G. 1951. Studies on lysogenesis I: The mode of phage liberation by lysogenic *Escherichia coli*. J. Bacteriol. 62:293-300.

Bickhart, D. M., Kolmogorov, M., Tseng, E., Portik, D. M., Korobeynikov, A., Tolstoganov, I., Uritskiy, G., Liachko, I., Sullivan, S. T., Shin, S. B., Zorea, A., Andreu, V. P., Panke-Buisse, K., Medema, M. H., Mizrahi, I., Pevzner, P. A., and Smith, T. P. L. 2022. Generating lineage-resolved, complete metagenome-assembled genomes from complex microbial communities. Nat. Biotechnol. 40:711-719.

Blin, K., Shaw, S., Augustijn, H. E., Reitz, Z. L., Biermann, F., Alanjary, M., Fetter, A., Terlouw, B. R., Metcalf, W. W., Helfrich, E. J. N., van Wezel, G. P., Medema, M. H., and Weber, T. 2023. antiSMASH 7.0: New and improved predictions for detection, regulation, chemical structures and visualisation. Nucleic. Acids. Res. 51:W46-W50.

Blin, K., Shaw, S., Vader, L., Szenei, J., Reitz, Z. L., Augustijn, H. E., Cediel-Becerra, J. D. D., de Crécy-Lagard, V., Koetsier, R. A., Williams, S. E., Cruz-Morales, P., Wongwas, S., Segurado Luchsinger, A. E., Biermann, F., Korenskaia, A., Zdouc, M. M., Meijer, D., Terlouw, B. R., van der Hooft, J. J. J., Ziemert, N., Helfrich, E. J. N., Masschelein, J., Corre, C., Chevrette, M. G., van Wezel, G. P., Medema, M. H., and Weber, T. 2025. antiSMASH 8.0: Extended gene cluster detection capabilities and analyses of chemistry, enzymology, and regulation. Nucleic Acids Res. 53:W32-W38.

Boratyn, G. M., Thierry-Mieg, J., Thierry-Mieg, D., Busby, B., and Madden, T. L. 2019. Magic-BLAST, an accurate RNA-seq aligner for long and short reads. BMC Bioinform. 20:405.

Bulgarelli, D., Schlaeppi, K., Spaepen, S., van Themaat, E. V. L., and Schulze-Lefert, P. 2013. Structure and functions of the bacterial microbiota of plants. Annu. Rev. Plant Biol. 64:807-838.

Burton, J. N., Liachko, I., Dunham, M. J., and Shendure, J. 2014. Species-level deconvolution of metagenome assemblies with Hi-C–based contact probability maps. G3 4:1339-1346.

Butler, M. I., Stockwell, P. A., Black, M. A., Day, R. C., Lamont, I. L., and Poulter, R. T. M. 2013. *Pseudomonas syringae* pv. *actinidiae* from recent outbreaks of kiwifruit bacterial canker belong to different clones that originated in China. PLoS One 8:e57464.

Byers, A. K., Waipara, N., Condron, L., and Black, A. 2024. The impacts of ecological disturbances on the diversity of biosynthetic gene clusters in kauri (*Agathis australis*) soil. Environ. Microbiome 19:69.

Cai, J., Jiang, Y., Ritchie, E. S., Macho, A. P., Yu, F., and Wu, D. 2023. Manipulation of plant metabolism by pathogen effectors: More than just food. FEMS Microbiol. Rev. 47:fuad007.

Callahan, B. J., McMurdie, P. J., Rosen, M. J., Han, A. W., Johnson, A. J. A., and Holmes, S. P. 2016. DADA2: High-resolution sample inference from Illumina amplicon data. Nat. Methods 13:581-583.

Camacho, C., Coulouris, G., Avagyan, V., Ma, N., Papadopoulos, J., Bealer, K., and Madden, T. L. 2009. BLAST+: Architecture and applications. BMC Bioinform. 10:421.

Cellini, A., Buriani, G., Correia, C., Fiorentini, L., Vandelle, E., Polverari, A., Santos, C., Vanneste, J. L., and Spinelli, F. 2022. Host-specific signal perception by PsaR2 LuxR solo induces *Pseudomonas syringae* pv. *actinidiae* virulence traits. Microbiol. Res. 260:127048.

Cellini, A., Donati, I., Farneti, B., Khomenko, I., Buriani, G., Biasioli, F., Cristescu, S. M., and Spinelli, F. 2021. A breach in plant defences: *Pseudomonas syringae* pv. *actinidiae* targets ethylene signalling to overcome *Actinidia chinensis* pathogen responses. Int. J. Mol. Sci. 22:4375.

Chaudhry, V., Runge, P., Sengupta, P., Doehlemann, G., Parker, J. E., and Kemen, E. 2021. Shaping the leaf microbiota: Plant–microbe–microbe interactions. J. Exp. Bot. 72:36-56.

Chen, T., Nomura, K., Wang, X., Sohrabi, R., Xu, J., Yao, L., Paasch, B. C., Ma, L., Kremer, J., Cheng, Y., Zhang, L., Wang, N., Wang, E., Xin, X.-F., and He, S. Y. 2020. A plant genetic network for preventing dysbiosis in the phyllosphere. Nature 580:653-657.

Colombi, E., Straub, C., Kuenzel, S., Templeton, M. D., McCann, H. C., and Rainey, P. B. 2017. Evolution of copper resistance in the kiwifruit pathogen *Pseudomonas syringae* pv. *actinidiae* through acquisition of integrative conjugative elements and plasmids. Environ. Microbiol. 19:819-832.

Cook, D. E., Mesarich, C. H., and Thomma, B. P. H. J. 2015. Understanding plant immunity as a surveillance system to detect invasion. Annu. Rev. Phytopathol. 53:541-563.

Cunty, A., Poliakoff, F., Rivoal, C., Cesbron, S., Fischer-Le Saux, M., Lemaire, C., Jacques, M. A., Manceau, C., and Vanneste, J. L. 2015. Characterization of *Pseudomonas syringae* pv. *actinidiae* (Psa) isolated from France and assignment of Psa biovar 4 to a de novo pathovar: *Pseudomonas syringae* pv. *actinidifoliorum* pv. nov. Plant Pathol. 64:582-596.

Datson, P., Nardozza, S., Manako, K., Herrick, J., Martinez-Sanchez, M., Curtis, C., and Montefiori, M. 2015. Monitoring the *Actinidia* germplasm for resistance to *Pseudomonas syringae* pv. *actinidiae*. Acta Hortic. 1095:181-184.

Davis, N. M., Proctor, D. M., Holmes, S. P., Relman, D. A., and Callahan, B. J. 2018. Simple statistical identification and removal of contaminant sequences in marker-gene and metagenomics data. Microbiome 6:226.

Diallo, M. D., Monteil, C. L., Vinatzer, B. A., Clarke, C. R., Glaux, C., Guilbaud, C., Desbiez, C., and Morris, C. E. 2012. *Pseudomonas syringae* naturally lacking the canonical type III secretion system are ubiquitous in nonagricultural habitats, are phylogenetically diverse and can be pathogenic. ISME J. 6:1325-1335.

Dillon, M. M., Almeida, R. N. D., Laflamme, B., Martel, A., Weir, B. S., Desveaux, D., and Guttman, D. S. 2019. Molecular evolution of *Pseudomonas syringae* type III secreted effector proteins. Front. Plant Sci. 10:418.

Donati, I., Cellini, A., Sangiorgio, D., Vanneste, J. L., Scortichini, M., Balestra, G. M., and Spinelli, F. 2020. *Pseudomonas syringae* pv. *actinidiae*: Ecology, infection dynamics and disease epidemiology. Microb. Ecol. 80:81-102.

Dorn-In, S., Bassitta, R., Schwaiger, K., Bauer, J., and Hölzel, C. S. 2015. Specific amplification of bacterial DNA by optimized so-called universal bacterial primers in samples rich of plant DNA. J. Microbiol. Methods 113: 50-56.

Drew, G. C., Stevens, E. J., and King, K. C. 2021. Microbial evolution and transitions along the parasite–mutualist continuum. Nat. Rev. Microbiol. 19:623-638.

Ehau-Taumaunu, H., and Hockett, K. L. 2023. Passaging phyllosphere microbial communities develop suppression towards bacterial speck disease in tomato. Phytobiomes J. 7:233-243.

Ehau-Taumaunu, H., and Hockett, K. L. 2022. The plant host environment influences competitive interactions between bacterial pathogens. Environ. Microbiol. Rep. 14:785-794.

Everett, K. R., Taylor, R. K., Romberg, M. K., Rees-George, J., Fullerton, R. A., Vanneste, J. L., and Manning, M. A. 2011. First report of *Pseudomonas syringae* pv. *actinidiae* causing kiwifruit bacterial canker in New Zealand. Australas. Plant Dis. Notes 6:67-71.

Ewels, P., Magnusson, M., Lundin, S., and Käller, M. 2016. MultiQC: Summarize analysis results for multiple tools and samples in a single report. Bioinformatics 32:3047-3048.

Fujikawa, T., and Sawada, H. 2019. Genome analysis of *Pseudomonas syringae* pv. *actinidiae* biovar 6, which produces the phytotoxins, phaseolotoxin and coronatine. Sci. Rep. 9:3836.

Gitaitis, R. D., Sasser, M. J., Beaver, R. W., McInnes, T. B., and Stall, R. E. 1987. Pectolytic xanthomonads in mixed infections with *Pseudomonas syringae* pv. *syringae*, *P. syringae* pv. *tomato*, and *Xanthomonas campestris* pv. *vesicatoria* in tomato and pepper transplants. Phytopathology 77:611-615.

González, A. J., Díaz, D., Ciordia, M., and Landeras, E. 2024. Occurrence of *Pseudomonas syringae* pvs. actinidiae, actinidifoliorum and other *P. syringae* strains on kiwifruit in northern Spain. Life 14:208.

Grenz, K., Chia, K.-S., Turley, E. K., Tyszka, A. S., Atkinson, R. E., Reeves, J., Vickers, M., Rejzek, M., Walker, J. F., and Carella, P. 2025. A necrotizing toxin enables *Pseudomonas syringae* infection across evolutionarily divergent plants. Cell Host Microbe 33:20-29.

Hemara, L. M., Chatterjee, A., Yeh, S.-M., Chen, R. K. Y., Hilario, E., Lievre, L. L., Crowhurst, R. N., Bohne, D., Arshed, S., Patterson, H. R., Barrett-Manako, K., Thomson, S., Allan, A. C., Brendolise, C., Chagné, D., Templeton, M. D., Tahir, J., and Jayaraman, J. 2025a. Identification and characterization of innate immunity in *Actinidia melanandra* in response to *Pseudomonas syringae* pv. *actinidiae*. Plant Cell Environ. 48:1037-1050.

Hemara, L. M., Hoyte, S. M., Arshed, S., Schipper, M. M., Wood, P. N., Marshall, S. L., Andersen, M. T., Patterson, H. R., Vanneste, J. L., Peacock, L., Jayaraman, J., and Templeton, M. D. 2025b. Genomic biosurveillance of the kiwifruit pathogen *Pseudomonas syringae* pv. *actinidiae* biovar 3 reveals adaptation to selective pressures in New Zealand orchards. Mol. Plant Pathol. 26:e70056.

Hemara, L. M., Jayaraman, J., Sutherland, P. W., Montefiori, M., Arshed, S., Chatterjee, A., Chen, R., Andersen, M. T., Mesarich, C. H., van der Linden, O., Yoon, M., Schipper, M. M., Vanneste, J. L., Brendolise, C., and Templeton, M. D. 2022. Effector loss drives adaptation of *Pseudomonas syringae* pv. *actinidiae* biovar 3 to *Actinidia arguta*. PLoS Pathog. 18:e1010542.

Hirano, S. S., and Upper, C. D. 2000. Bacteria in the leaf ecosystem with emphasis on *Pseudomonas syringae*—A pathogen, ice nucleus, and epiphyte. Microbiol. Mol. Biol. Rev. 64:624-653.

Hoffbeck, C., Middleton, D. M. R. L., Nelson, N. J., and Taylor, M. W. 2023. 16S rRNA gene-based meta-analysis of the reptile gut microbiota reveals environmental effects, host influences and a limited core microbiota. Mol. Ecol. 32:6044-6058.

Hosni, T., Moretti, C., Devescovi, G., Suarez-Moreno, Z. R., Fatmi, M. B., Guarnaccia, C., Pongor, S., Onofri, A., Buonaurio, R., and Venturi, V. 2011. Sharing of quorum-sensing signals and role of interspecies communities in a bacterial plant disease. ISME J. 5:1857-1870.

Howe, A., Stopnisek, N., Dooley, S. K., Yang, F., Grady, K. L., and Shade, A. 2023. Seasonal activities of the phyllosphere microbiome of perennial crops. Nat. Commun. 14:1039.

Ishiga, T., Sakata, N., Usuki, G., Nguyen, V. T., Gomi, K., and Ishiga, Y. 2023. Large–scale transposon mutagenesis reveals type III secretion effector HopR1 is a major virulence factor in *Pseudomonas syringae* pv. *actinidiae*. Plants 12:141.

Jayaraman, J., Yoon, M., Applegate, E. R., Stroud, E. A., and Templeton, M. D. 2020. AvrE1 and HopR1 from *Pseudomonas syringae* pv. *actinidiae* are additively required for full virulence on kiwifruit. Mol. Plant Pathol. 21:1467-1480.

Jayaraman, J., Yoon, M., Hemara, L. M., Bohne, D., Tahir, J., Chen, R. K. Y., Brendolise, C., Rikkerink, E. H. A., and Templeton, M. D. 2023. Contrasting effector profiles between bacterial colonisers of kiwifruit reveal redundant roles converging on PTI-suppression and RIN4. New Phytol. 238:1605-1619.

Johnson, M., Zaretskaya, I., Raytselis, Y., Merezhuk, Y., McGinnis, S., and Madden, T. L. 2008. NCBI BLAST: A better web interface. Nucleic Acids Res. 36:W5-W9.

Kassambara, A. 2017. ggpubr: 'ggplot2' Based Publication Ready Plots. https://CRAN.R-project.org/package=ggpubr

Kusstatscher, P., Wicaksono, W. A., Bergna, A., Cernava, T., Bergau, N., Tissier, A., Hause, B., and Berg, G. 2020. Trichomes form genotype-specific microbial hotspots in the phyllosphere of tomato. Environ. Microbiome 15:17.

Lahti, L., and Shetty, S. 2017. microbiome. R package. Bioconductor. https://doi.org/10.18129/B9.bioc.microbiome

Lamichhane, J. R., and Venturi, V. 2015. Synergisms between microbial pathogens in plant disease complexes: A growing trend. Front. Plant Sci. 6:385.

Leveau, J. H. J. 2006. Microbial communities in the phyllosphere. Pages 334-367 in: Biology of the Plant Cuticle. M. Riederer and C. Müller, eds. Blackwell, Oxford, United Kingdom.

Lindeberg, M., Cunnac, S., and Collmer, A. 2012. *Pseudomonas syringae* type III effector repertoires: Last words in endless arguments. Trends Microbiol. 20:199-208.

Lindow, S. E., and Brandl, M. T. 2003. Microbiology of the phyllosphere. Appl. Environ. Microbiol. 69:1875-1883.

Liu, Y., Li, D., Zhang, Q., Song, C., Zhong, C., Zhang, X., Wang, Y., Yao, X., Wang, Z., Zeng, S., Wang, Y., Guo, Y., Wang, S., Li, X., Li, L., Liu, C., McCann, H. C., He, W., Niu, Y., Chen, M., Du, L., Gong, J., Datson,

P. M., Hilario, E., and Huang, H. 2017. Rapid radiations of both kiwifruit hybrid lineages and their parents shed light on a two-layer mode of species diversification. New Phytol. 215:877-890.

Louisson, Z., Ranjard, L., Buckley, H. L., Case, B. S., and Lear, G. 2023. Soil bacterial community composition is more stable in kiwifruit orchards relative to phyllosphere communities over time. Environ. Microbiome 18:71.

Marbouty, M., Cournac, A., Flot, J.-F., Marie-Nelly, H., Mozziconacci, J., and Koszul, R. 2014. Metagenomic chromosome conformation capture (meta3C) unveils the diversity of chromosome organization in microorganisms. eLife 3:e03318.

Mayer, T., Mari, A., Almario, J., Murillo-Roos, M., Syed M. Abdullah, H., Dombrowski, N., Hacquard, S., Kemen, E. M., and Agler, M. T. 2021. Obtaining deeper insights into microbiome diversity using a simple method to block host and nontargets in amplicon sequencing. Mol. Ecol. Resour. 21: 1952-1965.

McAtee, P. A., Brian, L., Curran, B., van der Linden, O., Nieuwenhuizen, N. J., Chen, X., Henry-Kirk, R. A., Stroud, E. A., Nardozza, S., Jayaraman, J., Rikkerink, E. H. A., Print, C. G., Allan, A. C., and Templeton, M. D. 2018. Re-programming of *Pseudomonas syringae* pv. *actinidiae* gene expression during early stages of infection of kiwifruit. BMC Genomics 19:822.

McCann, H. C., Li, L., Liu, Y., Li, D., Pan, H., Zhong, C., Rikkerink, E. H. A., Templeton, M. D., Straub, C., Colombi, E., Rainey, P. B., and Huang, H. 2017. Origin and evolution of the kiwifruit canker pandemic. Genome Biol. Evol. 9:932-944.

McCann, H. C., Rikkerink, E. H. A., Bertels, F., Fiers, M., Lu, A., Rees-George, J., Andersen, M. T., Gleave, A. P., Haubold, B., Wohlers, M. W., Guttman, D. S., Wang, P. W., Straub, C., Vanneste, J., Rainey, P. B., and Templeton, M. D. 2013. Genomic analysis of the kiwifruit pathogen *Pseudomonas syringae* pv. *actinidiae* provides insight into the origins of an emergent plant disease. PLoS Pathog. 9:e1003503.

McMurdie, P. J., and Holmes, S. 2013. phyloseq: An R package for reproducible interactive analysis and graphics of microbiome census data. PLoS One 8:e61217.

Michelotti, V., Lamontanara, A., Buriani, G., Orrù, L., Cellini, A., Donati, I., Vanneste, J. L., Cattivelli, L., Tacconi, G., and Spinelli, F. 2018. Comparative transcriptome analysis of the interaction between *Actinidia chinensis* var. *chinensis* and *Pseudomonas syringae* pv. *actinidiae* in absence and presence of acibenzolar-S-methyl. BMC Genomics 19:585.

Millett, F., Standish, J., Scanley, J., Miller, K., Inguagiato, J., Zuverza-Mena, N., Abril, M., Robinson, V., Li, Y., Sundin, G. W., and Zeng, Q. 2025. The fire blight pathogen *Erwinia amylovora* enters apple leaves through naturally occurring wounds from the abscission of trichomes. Plant J. 123:e70472.

Morris, C. E. 2002. Phyllosphere. In: Encyclopedia of Life Sciences. John Wiley & Sons, Ltd., Oxford, United Kingdom. https://doi.org/10.1038/npg.els.0000400

Morris, C. E., Lamichhane, J. R., Nikolić, I., Stanković, S., and Moury, B. 2019. The overlapping continuum of host range among strains in the *Pseudomonas syringae* complex. Phytopathol. Res. 1:4.

Morris, C. E., Sands, D. C., Vinatzer, B. A., Glaux, C., Guilbaud, C., Buffière, A., Yan, S., Dominguez, H., and Thompson, B. M. 2008. The life history of the plant pathogen *Pseudomonas syringae* is linked to the water cycle. ISME J. 2:321-334.

Nardozza, S., Boldingh, H. L., Osorio, S., Höhne, M., Wohlers, M., Gleave, A. P., MacRae, E. A., Richardson, A. C., Atkinson, R. G., Sulpice, R., Fernie, A. R., and Clearwater, M. J. 2013. Metabolic analysis of kiwifruit (*Actinidia deliciosa*) berries from extreme genotypes reveals hallmarks for fruit starch metabolism. J. Exp. Bot. 64:5049-5063.

Nomura, K., Andreazza, F., Cheng, J., Dong, K., Zhou, P., and He, S. Y. 2023. Bacterial pathogens deliver water- and solute-permeable channels to plant cells. Nature 621:586-591.

Oksanen, J., Simpson, G. L., Blanchet, F. G., Kindt, R., Legendre, P., Minchin, P. R., O'Hara, R. B., Solymos, P., Stevens, M. H. H., Szoecs, E., Wagner, H., Barbour, M., Bedward, M., Bolker, B., Borcard, D., Borman, T., Carvalho, G., Chirico, M., Caceres, M. D., Durand, S., Evangelista, H. B. A., FitzJohn, R., Friendly, M., Furneaux, B., Hannigan, G., Hill, M. O., Lahti, L., Martino, C., McGlinn, D., Ouellette, M.-H., Cunha, E. R., Smith, T., Stier, A., Ter Braak, C. J. F., and Weedon, J. 2024. vegan: Community Ecology Package. https://CRAN.R-project.org/package=vegan

Paasch, B. C., Sohrabi, R., Kremer, J. M., Nomura, K., Cheng, Y. T., Martz, J., Kvitko, B., Tiedje, J. M., and He, S. Y. 2023. A critical role of a eubiotic microbiota in gating proper immunocompetence in *Arabidopsis*. Nat. Plants 9:1468-1480.

Peñuelas, J., and Terradas, J. 2014. The foliar microbiome. Trends Plant Sci. 19:278-280.

Poulter, R. T. M., Ho, J., Handley, T., Taiaroa, G., and Butler, M. I. 2018. Comparison between complete genomes of an isolate of *Pseudomonas syringae* pv. *actinidiae* from Japan and a New Zealand isolate of the pandemic lineage. Sci. Rep. 8:10915.

Purahong, W., Orrù, L., Donati, I., Perpetuini, G., Cellini, A., Lamontanara, A., Michelotti, V., Tacconi, G., and Spinelli, F. 2018. Plant microbiome and its link to plant health: Host species, organs and *Pseudomonas syringae* pv. *actinidiae* infection shaping bacterial phyllosphere communities of kiwifruit plants. Front. Plant Sci. 9:1563.

R Core Team. 2024. R: A Language and Environment for Statistical Computing. R Foundation for Statistical Computing, Vienna, Austria.

Rees-George, J., Vanneste, J. L., Cornish, D. A., Pushparajah, I. P. S., Yu, J., Templeton, M. D., and Everett, K. R. 2010. Detection of *Pseudomonas syringae* pv. *actinidiae* using polymerase chain reaction (PCR) primers based on the 16S-23S rDNA intertranscribed spacer region and comparison with PCR primers based on other gene regions. Plant Pathol. 59:453-464.

Richardson, A. C., Burdon, J. N., and Ferguson, A. R. 2023. Kiwifruit: Botany, Production and Uses. CABI, Wallingford, United Kingdom.

Rufián, J. S., Macho, A. P., Corry, D. S., Mansfield, J. W., Ruiz-Albert, J., Arnold, D. L., and Beuzón, C. R. 2018. Confocal microscopy reveals *in planta* dynamic interactions between pathogenic, avirulent and non-pathogenic *Pseudomonas syringae* strains. Mol. Plant Pathol. 19:537-551.

Ruiz-Bedoya, T., Wang, P. W., Desveaux, D., and Guttman, D. S. 2023. Cooperative virulence via the collective action of secreted pathogen effectors. Nat. Microbiol. 8:640-650.

Sacristán, S., and García-Arenal, F. 2008. The evolution of virulence and pathogenicity in plant pathogen populations. Mol. Plant Pathol. 9:369-384.

Sadhukhan, S., Jacques, M.-A., and Potnis, N. 2024. Influence of co-occurring weakly pathogenic bacterial species on bacterial spot disease dynamics on tomato. Plant Dis. 108:190-199.

Sawada, H., and Fujikawa, T. 2019. Genetic diversity of *Pseudomonas syringae* pv. *actinidiae*, pathogen of kiwifruit bacterial canker. Plant Pathol. 68:1235-1248.

Schlechter, R. O., Kear, E. J., Bernach, M., Remus, D. M., and Remus-Emsermann, M. N. P. 2023. Metabolic resource overlap impacts competition among phyllosphere bacteria. ISME J. 17:1445-1454.

Seemann, T. 2014. Prokka: Rapid prokaryotic genome annotation. Bioinformatics 30:2068-2069.

Smith, W. P. J., Vettiger, A., Winter, J., Ryser, T., Comstock, L. E., Basler, M., and Foster, K. R. 2020. The evolution of the type VI secretion system as a disintegration weapon. PLoS Biol. 18:e3000720.

Sohrabi, R., Paasch, B. C., Liber, J. A., and He, S. Y. 2023. Phyllosphere microbiome. Annu. Rev. Plant Biol. 74:539-568.

Stamatakis, A. 2014. RAxML version 8: A tool for phylogenetic analysis and post-analysis of large phylogenies. Bioinformatics 30:1312-1313.

Straub, C., Colombi, E., Li, L., Huang, H., Templeton, M. D., McCann, H. C., and Rainey, P. B. 2018. The ecological genetics of *Pseudomonas syringae* from kiwifruit leaves. Environ. Microbiol. 20:2066-2084.

Su, P., Kang, H., Peng, Q., Wicaksono, W. A., Berg, G., Liu, Z., Ma, J., Zhang, D., Cernava, T., and Liu, Y. 2024. Microbiome homeostasis on rice leaves is regulated by a precursor molecule of lignin biosynthesis. Nat. Commun. 15:23.

Tonkin-Hill, G., MacAlasdair, N., Ruis, C., Weimann, A., Horesh, G., Lees, J. A., Gladstone, R. A., Lo, S., Beaudoin, C., Floto, R. A., Frost, S. D. W., Corander, J., Bentley, S. D., and Parkhill, J. 2020. Producing polished prokaryotic pangenomes with the Panaroo pipeline. Genome Biol. 21:180.

Tyson, J. L., Manning, M. A., Mellow, K. D., and Vergara, M. J. 2018. *Pseudomonas syringae* pv. *actinidiae* survival in point-inoculated kiwifruit vines. N. Z. Plant Prot. 71:45-50.

Vacher, C., Hampe, A., Porté, A. J., Sauer, U., Compant, S., and Morris, C. E. 2016. The phyllosphere: Microbial jungle at the plant–climate interface. Annu. Rev. Ecol. Evol. Syst. 47:1-24.

Vadillo-Dieguez, A., Zeng, Z., Mansfield, J. W., Grinberg, N. F., Lynn, S. C., Gregg, A., Connell, J., Harrison, R. J., Jackson, R. W., and Hulin, M. T. 2024. Genetic dissection of the tissue-specific roles of type III effectors and phytotoxins in the pathogenicity of *Pseudomonas syringae* pv. *syringae* to cherry. Mol. Plant Pathol. 25:e13451.

Visnovsky, S. B., Marroni, M. V., Pushparajah, S., Everett, K. R., Taylor, R. K., Vinatzer, B. A., and Pitman, A. R. 2019. Using multilocus sequence analysis to distinguish pathogenic from saprotrophic strains of *Pseudomonas* from stone fruit and kiwifruit. Eur. J. Plant Pathol. 155:643-658.

Vlková-Žlebková, M., Yuen, F. W., and McCann, H. C. 2024. Evolving archetypes: Learning from pathogen emergence on a nonmodel host. Annu. Rev. Phytopathol. 62:49-68.

Vorholt, J. A. 2012. Microbial life in the phyllosphere. Nat. Rev. Microbiol. 10:828-840.

Wagner, M. R., Busby, P. E., and Balint-Kurti, P. 2020. Analysis of leaf microbiome composition of near-isogenic maize lines differing in broad-spectrum disease resistance. New Phytol. 225:2152-2165.

Wang, N. R., Wiesmann, C. L., Melnyk, R. A., Hossain, S. S., Chi, M.-H., Martens, K., Craven, K., and Haney, C. H. 2022. Commensal *Pseudomonas fluorescens* strains protect *Arabidopsis* from closely related *Pseudomonas* pathogens in a colonization-dependent manner. mBio 13: e02892-21.

Warring, S. L., Malone, L. M., Jayaraman, J., Easingwood, R. A., Rigano, L. A., Frampton, R. A., Visnovsky, S. B., Addison, S. M., Hernandez, L., Pitman, A. R., Lopez Acedo, E., Kleffmann, T., Templeton, M. D., Bostina, M., and Fineran, P. C. 2022. A lipopolysaccharide-dependent phage infects a pseudomonad phytopathogen and can evolve to evade phage resistance. Environ. Microbiol. 24:4834-4852.

Wickham, H. 2016. ggplot2: Elegant Graphics for Data Analysis. Springer Science+Business Media, New York, NY.

Wickham, H., Averick, M., Bryan, J., Chang, W., D'Agostino McGowan, L., François, R., Grolemund, G., Hayes, A., Henry, L., Hester, J., Kuhn, M., Pedersen, T. L., Miller, E., Bache, S. M., Müller, K., Ooms, J., Robinson, D., Seidel, D. P., Spinu, V., Takahashi, K., Vaughan, D., Wilke, C., Woo, K., and Yutani, H. 2019. Welcome to the Tidyverse. J. Open Source Softw. 4: 1686.

Wiesmann, C. L., Wang, N. R., Zhang, Y., Liu, Z., and Haney, C. H. 2022. Origins of symbiosis: Shared mechanisms underlying microbial pathogenesis, commensalism and mutualism of plants and animals. FEMS Microbiol. Rev. 47:fuac048.

Xin, X.-F., Kvitko, B., and He, S. Y. 2018. *Pseudomonas syringae*: What it takes to be a pathogen. Nat. Rev. Microbiol. 16:316-328.

Yang, Z., Liu, T., Fan, J., Chen, Y., Wu, S., Li, J., Liu, Z., Yang, Z., Li, L., Liu, S., Yang, H., Yin, H., Meng, D., and Tang, Q. 2024. Biocontrol agents modulate phyllosphere microbiota interactions against pathogen *Pseudomonas syringae*. Environ. Sci. Ecotechnol. 21:100431.

Yu, G., Smith, D. K., Zhu, H., Guan, Y., and Lam, T. T.-Y. 2017. ggtree: An R package for visualization and annotation of phylogenetic trees with their covariates and other associated data. Methods Ecol. Evol. 8:28-36.

Zhang, J., Zhou, M., Liu, W., Nie, J., and Huang, L. 2022. *Pseudomonas syringae* pv. *actinidiae* effector HopAU1 interacts with calcium-sensing receptor to activate plant immunity. Int. J. Mol. Sci. 23:508.

Zhao, Z., Chen, J., Gao, X., Zhang, D., Zhang, J., Wen, J., Qin, H., Guo, M., and Huang, L. 2019. Comparative genomics reveal pathogenicity-related loci in *Pseudomonas syringae* pv. *actinidiae* biovar 3. Mol. Plant Pathol. 20:923-942.